Universidad del Desarrollo
Facultad de Gobierno

Complex Oscillatory Dynamics in Neural Populations Using Map-Based Models

By: VICTOR JULIO MARQUEZ RODRIGUEZ

Thesis Submitted to the Facultad de Gobierno

Universidad del Desarrollo

to pursue the Degree of Doctor in Ciencias de la Complejidad Social.

Supervisors:

Main Supervisor: Dr. Pablo Billeke

Co-Supervisor: Dr. María Paz Raveau

Co-Supervisor: Dr. Patricia Soto-Icaza

July 2025

Contents

List of Figures

Summary

This thesis explores the emergence of complex oscillatory dynamics in neuronal populations, focusing on key phenomena such as chimera states, phase-amplitude coupling (PAC), and metastability. Neural oscillations play a fundamental role in coordinating brain functions, facilitating information integration, and supporting cognitive processes. Understanding how these oscillatory dynamics emerge requires investigating both the causal interactions shaping neural activity and the influence of structural organization on complex oscillatory features.

To address this inquiry, we have employed a two-stage computational modeling approach. In the first stage, a system of two populations of map-based neurons interacting through mean-field coupling was developed to analyze synchronization states and quantify information flow within chimera states. The second stage introduced a more biologically realistic model by incorporating synaptic interactions and a connectivity network derived from cortical tissue, allowing the exploration of how these structural factors influenced the emergence of complex oscillatory features such as PAC and metastability.

We have found that chimera states exhibited a well defined directional flow of information, from the desynchronized population to the synchronized one, offering insights into conditions such as epilepsy and autism. Furthermore, we have observed that incorporating realistic cortical connectivity enhanced PAC and metastability, emphasizing the role of cortical layer organization in shaping oscillatory frequency bands and adaptive brain dynamics.

By integrating computational modeling with map-based neuron models and experimental insights, this work aims to contribute to a better understanding of the dynamic oscillatory features of neural activity and their relevance to both normal and pathological brain states.

1. Introduction

From its origins, starting with the studies conducted and published in the 1920s by Berger (1929), the study and characterization of rhythmic patterns in neural activity using various methods have continuously advanced our understanding of the brain, both from clinical and research perspectives (Mulert and Lemieux, 2010; Niedermeyer et al., 2011; Nunez, 1981). Neural oscillations are essential for coordinating brain function, facilitating the integration of information across diverse neural networks and supporting complex cognitive tasks (Buzsaki and Draguhn, 2004). This rhythmic patterns emerge from the complex interactions between individual neurons and their synaptic networks (Wang, 2010).

Many oscillatory states consist of different dynamic components that can co-occur simultaneously and interact with one another, either within the same area or across different regions of the brain (Bick et al., 2020; Buzsáki et al., 2013). Chimera states provide an illustrative example, where synchronized and desynchronized activity coexist simultaneously within or between interconnected neural populations (Bansal et al., 2019). Likewise, phase-amplitude coupling (PAC) represents another form of interaction between different frequency rhythms, where a low-frequency rhythm modulates the amplitude of a high-frequency rhythm, illustrating the complex interplay of oscillations within the brain (Salimpour and Anderson, 2019).

Despite nearly a century of research on oscillations since their first experimental recordings, significant gaps remain in understanding how these complex dynamics emerge. A fundamental challenge in neuroscience is determining how

neuronal populations self-organize to generate and sustain complex oscillatory states. While single-neuron activity has been extensively characterized, a key open question remains: How do complex oscillatory dynamics emerge in neural populations?

To address this question, this work is structured in two stages. In the first stage, a model of two populations of map-based neurons interacting through their mean fields is proposed to define global coupling parameters that characterize synchronization states. The information flow between the synchronized and desynchronized neuron populations in a chimera state is then quantified. In the second stage, while maintaining the same local dynamics and having only one population of neurons, a more biologically plausible approach is adopted. This involves replacing mean field coupling with synaptic connections between map-based neurons and incorporating a connectivity network derived from cortical tissue of the human brain. This approach aims to study how these factors influence the emergence of complex oscillatory features, such as PAC and metastability. By studying these stages, we seek to better understand the mechanisms behind these oscillatory dynamics and their role in both normal and pathological brain functions.

To better understand the emergence of complex oscillatory features in the brain, it is crucial to study both the causal interactions that shape their dynamics and the influence of structural organization in neural networks. Chimera states, described initially in the main context of coupled oscillators, have been proposed to play a role in various brain processes, including unihemispheric sleep in different animal species and pathological conditions such as epileptic seizures (Glaze and Bahar, 2021; Lainscsek et al., 2019). In this way, it is valuable not only to identify chimeras and other collective states but also to explore the underlying causal interactions that may contribute to their emergence, particularly in the context of brain dynamics. In parallel, neuronal oscillations arise from intricate interactions across spatial scales, influenced by both network-level connectivity and the dynamics of individual neurons and synapses (Wang, 2010). Recent findings highlight the importance of cortical layer organization, where distinct frequency bands

emerge from specific cortical layers (Mendoza-Halliday et al., 2024), underscoring the need to explore how connectivity patterns shape key oscillatory properties such as PAC. Furthermore, since patterns like PAC facilitate spontaneous transitions between different states of neural activity (Sase and Kitajo, 2021), studying metastability is also crucial for understanding the brain's adaptive dynamics.

To explore these aspects, this study employs map-based neuron models as a key framework for analyzing complex neuronal dynamics. These models provide a computationally efficient and conceptually straightforward approach to simulating neuronal activity (Ibarz et al., 2011). Derived from integrate-and-fire frameworks, they offer a simplified yet robust representation of individual neuron behavior, capturing oscillatory and chaotic regimes with fewer dimensions compared to traditional differential equation models (Courbage and Nekorkin, 2010). Their discrete-time approach makes them particularly advantageous for studying large neuronal populations and emergent oscillatory phenomena, where computational efficiency and scalability are essential (Ibarz et al., 2011). Therefore, this work also attempts to further explore the capabilities and applications of map-based neuron models, assessing their effectiveness in capturing key aspects of neuronal dynamics and collective behavior.

The relevance of this study lies in its focus on understanding chimera states within neuronal dynamics to gain insights into neurological disorders and unihemispheric sleep. By investigating how these states influence brain function, we aim to uncover the underlying mechanisms that could explain abnormal neural synchronization patterns (Lainscsek et al., 2019). Additionally, we aim to improve our understanding of key oscillatory features as PAC and metastability, which have been observed in a variety of mammals and are fundamental for interregional brain communication during cognitive tasks (Billeke et al., 2020). Given the essential role of oscillatory patterns in neural communication, studying PAC will shed light on how brain regions coordinate to perform complex cognitive functions. Finally, the use of computational models provides a crucial theoretical tool to better interpret experimental data and simulate complex neural behavior, enhancing our

ability to make predictions about brain dynamics in both healthy and pathological states.

The remainder of this thesis is organized as follows. Chapter 2, titled *Chimera states and information transfer in interacting populations of map-based neurons*, focuses on the first research stage, while Chapter 3, titled *Impact of cortical connectivity on phase-amplitude coupling and metastability in neural networks*, explores the second stage. Both chapters follow a similar structure: first introducing the case study, then the model to be used, followed by the metrics and results, and finally, the conclusions. Lastly, Chapter 4 presents the general conclusions.

Bibliography

Bansal, K., Garcia, J. O., Tompson, S. H., Verstynen, T., Vettel, J. M., and Muldoon, S. F. (2019). Cognitive chimera states in human brain networks. *Science advances*, 5(4):eaau8535.

Berger, H. (1929). Über das elektroenkephalogramm des menschen. *Archiv für psychiatrie und nervenkrankheiten*, 87(1):527–570.

Bick, C., Goodfellow, M., Laing, C. R., and Martens, E. A. (2020). Understanding the dynamics of biological and neural oscillator networks through exact mean-field reductions: a review. *The Journal of Mathematical Neuroscience*, 10(1):9.

Billeke, P., Ossandon, T., Perrone-Bertolotti, M., Kahane, P., Bastin, J., Jerbi, K., Lachaux, J.-P., and Fuentealba, P. (2020). Human anterior insula encodes performance feedback and relays prediction error to the medial prefrontal cortex. *Cerebral Cortex*, 30(7):4011–4025.

Buzsaki, G. and Draguhn, A. (2004). Neuronal oscillations in cortical networks. *science*, 304(5679):1926–1929.

Buzsáki, G., Logothetis, N., and Singer, W. (2013). Scaling brain size, keeping timing: evolutionary preservation of brain rhythms. *Neuron*, 80(3):751–764.

Courbage, M. and Nekorkin, V. I. (2010). Map based models in neurodynamics. *International Journal of Bifurcation and Chaos*, 20(06):1631–1651.

Glaze, T. A. and Bahar, S. (2021). Neural synchronization, chimera states and sleep asymmetry. *Frontiers in Network Physiology*, 1:734332.

Ibarz, B., Casado, J. M., and Sanjuán, M. A. (2011). Map-based models in neuronal dynamics. *Physics reports*, 501(1-2):1–74.

Lainscsek, C., Rungratsameetaweemana, N., Cash, S. S., and Sejnowski, T. J. (2019). Cortical chimera states predict epileptic seizures. *Chaos: An Interdisciplinary Journal of Nonlinear Science*, 29(12):121106.

Mendoza-Halliday, D., Major, A. J., Lee, N., Lichtenfeld, M. J., Carlson, B., Mitchell, B., Meng, P. D., Xiong, Y., Westerberg, J. A., Jia, X., et al. (2024). A ubiquitous spectrolaminar motif of local field potential power across the primate cortex. *Nature Neuroscience*, 27(3):547–560.

Mulert, C. and Lemieux, L. (2010). *EEG-fMRI Physiological Basis, Technique, and Applications*.

Niedermeyer, E., Schomer, D., and da Silva, F. (2011). *Niedermeyer's Electroencephalography: Basic Principles, Clinical Applications, and Related Fields*. Niedermeyer's Electroencephalography: Basic Principles, Clinical Applications, and Related Fields. Wolters Kluwer Health/Lippincott Williams & Wilkins.

Nunez, P. (1981). *Electric Fields of the Brain: The Neurophysics of EEG*. Oxford University Press.

Salimpour, Y. and Anderson, W. S. (2019). Cross-frequency coupling based neuromodulation for treating neurological disorders. *Frontiers in neuroscience*, 13:125.

Sase, T. and Kitajo, K. (2021). The metastable brain associated with autistic-like traits of typically developing individuals. *PLOS Computational Biology*, 17(4):e1008929.

Wang, X.-J. (2010). Neurophysiological and computational principles of cortical rhythms in cognition. *Physiological reviews*, 90(3):1195–1268.

2. Chimera states and information transfer in interacting populations of map-based neurons

Abstract [1]

We investigate the synchronization behavior and the emergence of chimera states in a system of two interacting populations of maps possessing chaotic neural-like dynamics. We characterize four collective states on the space of coupling parameters of the system: complete synchronization, generalized synchronization, chimera states, and incoherence. We quantify the information exchange between the two neuron populations in chimera states. We have found a well-defined direction of the flow of information in chimera states, from the desynchronized population to the synchronized one. The incoherent population functions as a driver of the coherent neuron population in a chimera state. This feature is independent of the population sizes or population partitions. Our results yield insight into the communication mechanisms arising in brain processes such as unihemispheric sleep and epileptic seizures that have been associated to chimera states.

2.1 Introduction

The study of emergent collective states in systems composed of interacting populations of dynamical units is a relevant topic in complexity science. These systems have been investigated in many different areas, such as coupled networks of oscillators (Abrams et al., 2008; Montbrió et al., 2004), cohabitation of two biological species (Goel et al., 1971; Gomatam, 1974), competition of two languages (Patriarca and Leppänen, 2004), and neural networks (Maslennikov and Nekorkin, 2014; Stefanescu and Jirsa, 2008). In the context of neural systems, the study of interacting populations of dynamical units can be relevant to understand the functional dynamics of the brain (Cardanobile and Rotter, 2011; Magyar and Collins, 2015). Two-population models have been used in several studies, such as synchronization between oscillations emerging from separated cortical neuronal assemblies (Bibbig et al., 2002), neuronal information processing (Battaglia et al., 2012), and phase-coherence transitions between delay-coupled neuronal

[1] Published in Neural Computing and Applications on July 19, 2024.

populations (Barardi et al., 2014).

In many systems, collective behavior can be characterized as synchronization states arising from the interactions within and between populations. Recently, there has been great interest in the study of chimera states in dynamical networks (Abrams and Strogatz, 2004; Kuramoto and Battogtokh, 2002; Panaggio and Abrams, 2015; Zakharova, 2020). A chimera state consists of the coexistence of subsets of elements with synchronous and asynchronous dynamics in a spatiotemporal system. In a system of two interacting populations, a chimera state is manifested as one population displaying a synchronized behavior while the other remains desynchronized. Chimera states have been found in systems consisting of two interacting populations of oscillators (Abrams et al., 2008; Laing, 2010; Martens et al., 2016; Omelchenko et al., 2011; Premalatha et al., 2017), and in cross-cultural interactions of two social groups (González-Avella et al., 2014). They have been experimentally observed in two coupled populations of mechanical oscillators (Martens et al., 2013) and electrochemical oscillators (Tinsley et al., 2012).

Chimera states have been associated to brain processes such as unihemispheric sleep in various animal species including birds, aquatic mammals, and reptiles (Lesku et al., 2009; Rattenborg et al., 2000), as well as human electroencephalographic patterns in epileptic seizures (Andrzejak et al., 2016; Lainscsek et al., 2019). Chimera states have been found in a two-layer network brain model based on data from cerebral cortex (Kang et al., 2019) and in two-layer neuronal network with unidirectional inter-layer links (Li et al., 2019). Chimeras in neural systems have been mostly studied in models of coupled differential equations, such as the Hodgkin-Huxley model (Glaze et al., 2016), the Hindmarsh-Rose model (Bera et al., 2016; Glaze and Bahar, 2021; Hizanidis et al., 2016), and the Fitzhugh-Nagumo model (Essaki Arumugam and Spano, 2015; Omelchenko et al., 2015). More recently, chimera states have been reported in networks with neural-type local dynamics described by the Rulkov time-discrete map (Mehrabbeik et al., 2021; Rybalova et al., 2019).

In many situations it is important not only to characterize chimeras or other collective states, but also to understand the causal relationships between the constituent parts of a system that lead to such behaviors. In particular, information transfer measures have been proven useful to quantify drive-response causal relationships between subsystems and functional structures in diverse complex systems (Bossomaier et al., 2016). For example, the emergence of nontrivial collective behavior in chaotic dynamical networks has been associated to the flow of information from global to local scales (Cisneros et al., 2002). Transfer entropy methods have been widely employed in neuroscience to evaluate interdependence between electroencephalographic data sets (Wibral et al., 2014). Such measures allow, for instance, to evaluate coupling directions (Li et al., 2020) and connectivity (Ursino et al., 2020) between different regions of the brain.

In this article, we investigate the emergence of synchronization and chimera states in a system of two interacting populations of chaotic maps possessing neural-like dynamics. We characterize various synchronization states that arise in the system: complete synchronization, generalized synchronization, chimera states, and incoherence. Specifically, we address the question: who is the driver in a chimera state in neuron dynamical networks? We quantify the information flow between the synchronized and desynchronized neuron populations in a chimera state by employing the information transfer measure of Schreiber (Schreiber, 2000) in order to gain insight into the communication mechanisms associated to pathologies in the brain. We compare the information transfer between the mean fields of the two populations in chimera states. Our approach is simpler than methods based on delayed mutual information and Poincaré sections used to detect the flow of information in chimera states of phase oscillator networks (Deschle et al., 2019).

In Sec. 2.2, we introduce a model of two populations interacting through their mean fields and define the order parameters to characterize synchronization states. Section 2.3 describes the spatiotemporal patterns associated to the different collective synchronization states arising in the system. The collective states are char-

acterized on the phase space given by the coupling parameters of the system. Section 2.4 contains the calculation of the information transfer between the two neuron populations in a chimera state. We find a definitive direction of the flow of information from the desynchronized population to the synchronized one. Conclusions are presented in Sec. 2.5.

2.2 Model for two interacting populations of map-based neurons

Coupled map lattices or coupled map networks are spatiotemporal dynamical systems where space and time are discrete, but the state variables are continuous. They consist of a set of maps or iterative functions considered as nodes interacting on a lattice or network (Kaneko, 1984; Waller and Kapral, 1984). Coupled map networks have provided useful models for the study of diverse processes in spatially extended systems, with the advantage of being computationally efficient (Kaneko, 1993). The discrete-space character of coupled map systems makes them appropriate for the investigation of dynamics on nonuniform networks (Cosenza and Kapral, 1992).

Our system is composed of N maps possessing neuron dynamics, distributed into two populations denominated as α and β, with sizes N^α and N^β, respectively, such that $N = N^\alpha + N^\beta$. In order to model local excitable dynamics, we consider two-dimensional map-based neurons where the two variables may represent the membrane potential and outward ionic currents, respectively. We use the notation $[k]$ to indicate "or k". Then, the state of element $i[j] \in \alpha[\beta]$ at discrete time t is given by two variables $x_t^\alpha(i), y_t^\alpha(i)$ $[x_t^\beta(j), y_t^\beta(j)]$, where $i = 1, 2, \ldots, N^\alpha$; $j = 1, 2, \ldots, N^\beta$. We assume that each element within a population interacts with the mean field of that population and with the mean field of the other population. Mean-field coupling has been used in neural mass models (Breakspear and Jirsa, 2007; Naze et al., 2015; Stefanescu and Jirsa, 2008). Then, we define the dynamics of the two interacting populations of map-based neurons by the following coupled

map equations,

$$x^{\alpha}_{t+1}(i) = (1-\mu) f(x^{\alpha}_{t}(i), y^{\alpha}_{t}(i)) + \mu \bar{X}^{\alpha}_{t} + \epsilon \bar{X}^{\beta}_{t}, \quad (2.1)$$

$$y^{\alpha}_{t+1}(i) = g(x^{\alpha}_{t}(i), y^{\alpha}_{t}(i)); \quad (2.2)$$

$$x^{\beta}_{t+1}(j) = (1-\mu) f(x^{\beta}_{t}(j), y^{\beta}_{t}(j)) + \mu \bar{X}^{\beta}_{t} + \epsilon \bar{X}^{\alpha}_{t}, \quad (2.3)$$

$$y^{\beta}_{t+1}(j) = g(x^{\beta}_{t}(j), y^{\beta}_{t}(j)), \quad (2.4)$$

where the functions $f(x, y)$ and $g(x, y)$ describe the local dynamics, and parameters μ and ϵ characterize the strength of the intra-population and inter-population coupling, respectively. The mean fields of populations α and β at time t are defined, respectively, as

$$\bar{X}^{\alpha}_{t} = \frac{1}{N^{\alpha}} \sum_{i=1}^{N^{\alpha}} x^{\alpha}_{t}(i), \quad (2.5)$$

$$\bar{X}^{\beta}_{t} = \frac{1}{N^{\beta}} \sum_{j=1}^{N^{\beta}} x^{\beta}_{t}(j). \quad (2.6)$$

Figure (2.1) illustrates the system of two interacting populations of dynamical elements Eqs. (2.1)-(2.4).

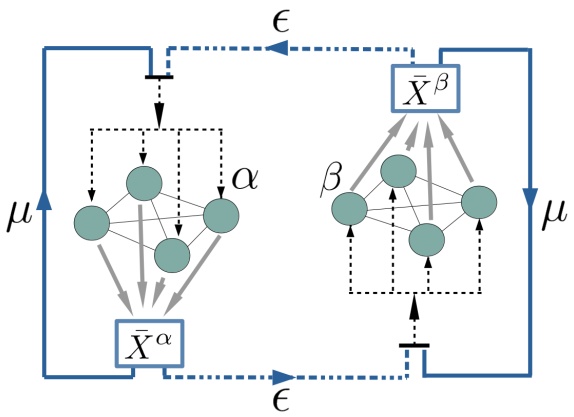

Figure 2.1: Scheme of two populations α and β reciprocally interacting through their mean fields. Any element in population $\alpha[\beta]$ interacts with: (i) all other elements in $\alpha[\beta]$ through the mean field $\bar{X}^{\alpha}$ $[\bar{X}^{\beta}]$ with coupling parameter μ, and (ii) the mean field $\bar{X}^{\beta}$ $[\bar{X}^{\alpha}]$ of population $\beta[\alpha]$ with strength ϵ.

Synchronization states for each population can be characterized by the following asymptotic time averages, after discarding a number of transients τ,

$$\langle \sigma^{\alpha} \rangle = \frac{1}{T-\tau} \sum_{t=\tau}^{T} \sigma_t^{\alpha}, \tag{2.7}$$

$$\langle \sigma^{\beta} \rangle = \frac{1}{T-\tau} \sum_{t=\tau}^{T} \sigma_t^{\beta}, \tag{2.8}$$

$$\langle \delta \rangle = \frac{1}{T-\tau} \sum_{t=\tau}^{T} |\bar{X}_t^{\alpha} - \bar{X}_t^{\beta}|, \tag{2.9}$$

where the instantaneous standard deviations of the distribution of state variables are defined by

$$\sigma_t^{\alpha} = \left[\frac{1}{N^{\alpha}} \sum_{i=1}^{N^{\alpha}} (x_t^{\alpha}(i) - \bar{X}_t^{\alpha})^2 \right]^{1/2}, \tag{2.10}$$

$$\sigma_t^{\beta} = \left[\frac{1}{N^{\beta}} \sum_{j=1}^{N^{\beta}} (x_t^{\beta}(j) - \bar{X}_t^{\beta})^2 \right]^{1/2}. \tag{2.11}$$

A collective state of synchronization within population α $[\beta]$ for the system represented by equations (2.1)-(2.3) and (2.3)-(2.4) takes place when $x_t^{\alpha[\beta]}(i) = x_t^{\alpha[\beta]}(k) = \bar{X}_t^{\alpha[\beta]}$ and $y_t^{\alpha[\beta]}(i) = y_t^{\alpha[\beta]}(k)$, $\forall i, k \in \alpha[\beta]$, sustained in time. Thus, a complete state of synchronization in population α is characterized by the condition $\langle \sigma^{\alpha} \rangle = 0$, and similarly population β is synchronized when $\langle \sigma^{\beta} \rangle = 0$. In numerical simulations, we set the criterion $\langle \sigma^{\alpha[\beta]} \rangle < 10^{-7}$ for synchronization of a population.

Different collective states of synchronization can be defined in the system Eqs. (2.1)-(2.4):

1. *Complete synchronization* (CS): when all elements within each population are synchronized with each other and with the elements of the other population. That is, $\langle \sigma^{\alpha} \rangle = 0$, $\langle \sigma^{\beta} \rangle = 0$, and $\langle \delta \rangle = 0$.

2. *Generalized Synchronization* (GS): when the elements within each popu-

lation are synchronized but not with the elements of the other population (Alvarez-Llamoza and Cosenza, 2008). That is, $\langle \sigma^{\alpha} \rangle = 0$ and $\langle \sigma^{\beta} \rangle = 0$, but $\langle \delta \rangle \neq 0$.

3. *Chimera state* (Q): when the elements in one population are synchronized but the elements in the other population are not. That is, $\langle \sigma^{\alpha} \rangle = 0$, $\langle \sigma^{\beta} \rangle \neq 0$, or viceversa, and $\langle \delta \rangle \neq 0$.

4. *Desynchronization* (D): none of the populations exhibits synchronization. This means, $\langle \sigma^{\alpha} \rangle \neq 0$ and $\langle \sigma^{\beta} \rangle \neq 0$.

We consider the two-dimensional map proposed by Rulkov (2002) as local neural dynamics, defined as

$$x_{t+1} = h(x_t, y_t), \tag{2.12}$$

$$y_{t+1} = y_t - \upsilon(x_t + 1) + \upsilon\gamma, \tag{2.13}$$

where x_t and y_t are the fast and slow variables. As for the two previous local maps, although these variables have not specific biological meaning, x_t can be interpreted as the transmembrane potential of a neuron, while y_t is a recovery or adaptation variable, where slow time evolution is given by small values of the parameter υ $(0 < \upsilon \ll 1)$.

To generate spiking and silent regimes, Eq. (3.1) employs a piecewise function $h(x, y)$ of the form

$$h(x,y) = \begin{cases} \varrho(1-x)^{-1} + y & \text{if} \quad x \leq 0, \\ \varrho + y & \text{if} \quad 0 < x < \varrho + y, \\ -1 & \text{if} \quad x \geq \varrho + y. \end{cases} \tag{2.14}$$

where γ and ϱ are control parameters that allow to select different regimes of temporal behavior of the model. Figure 2.2 shows the time evolution of the Rulkov map variables for parameter values $\upsilon = 0.001$, $\varrho = 4.6$ and $\gamma = 0.225$ which

correspond to the chaotic spiking region, as reported in (Shilnikov and Rulkov, 2003).

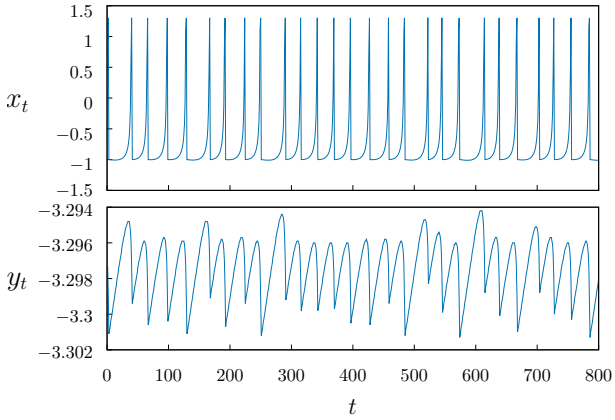

Figure 2.2: Time series of a single Rulkov map, Eqs. (3.1)-(3.2), with parameters $\upsilon = 0.001$, $\varrho = 4.6$, $\gamma = 0.225$.

2.3 Synchronization and chimera states

Figure 2.3 shows the asymptotic evolution of the variables $x_t^{\alpha}(i)$, $\forall i \in \alpha$, and $x_t^{\beta}(j)$, $\forall j \in \beta$ for the two interacting population model, Eqs. (2.1)-(2.4), with Rulkov local dynamics, Eqs. (3.1)-(3.2), for different values of coupling parameters μ and ϵ. Spatiotemporal patterns for complete synchronization, generalized synchronization, chimera state, and desynchronization are shown.

Figure 2.4 shows the collective synchronization states of the two population system, Eqs. (2.1)-(2.4), with local dynamics given by the Rulkov map, Eqs. (3.1)-(3.2), on the space of the coupling parameters (μ, ϵ). A complex structure is revealed in Fig. 2.4. Complete synchronization, generalized synchronization, disordered, and chimera states, characterized by the quantities $\langle \sigma^{\alpha} \rangle$, $\langle \sigma^{\beta} \rangle$, and $\langle \delta \rangle$ appear disperse over the parameter space (μ, ϵ).

To investigate the influence of asymmetry in the population sizes on the emergence of chimera states, we performed simulations for different partitions of N^{α} and N^{β}. Figure 2.5 shows chimera patterns for two different partitions and for the two local map-based neurons considered in this article. The relative sizes of

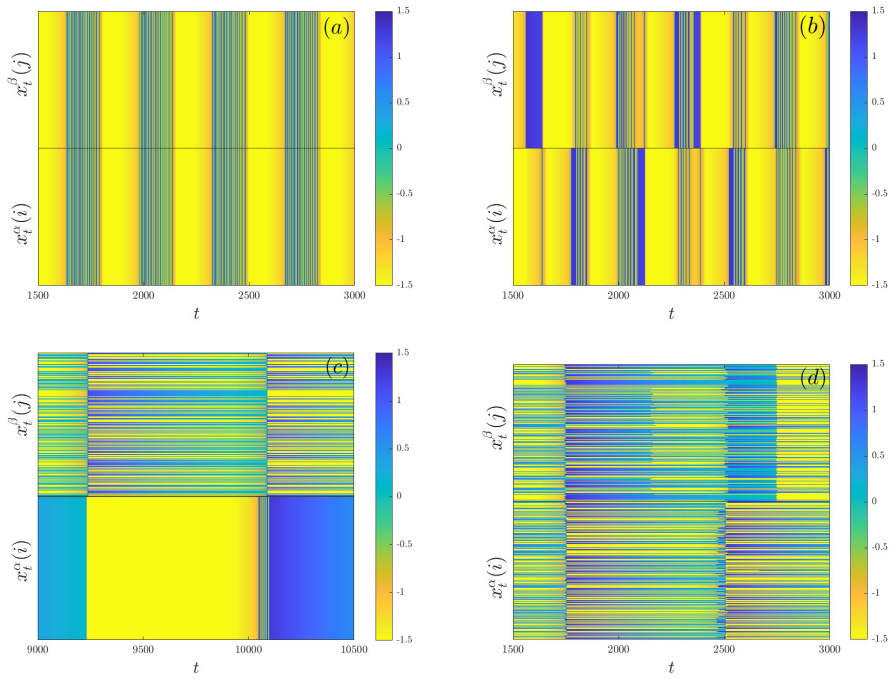

Figure 2.3: Spatiotemporal patterns for the two-population model, Eqs. (2.1)-(2.4), with local Rulkov dynamics, Eqs. (3.1)-(3.2). Population sizes $N^\alpha = N^\beta = 400$. Fixed parameters $\upsilon = 0.001$, $\varrho = 4.6$, $\gamma = 0.225$. (a) Synchronization ($\langle\sigma^\alpha\rangle = \langle\sigma^\beta\rangle = 0$, $\langle\delta\rangle = 0$)), $\mu = 0.08$ and $\epsilon = 0.04$. (b) Generalized synchronization ($\langle\sigma^\alpha\rangle = \langle\sigma^\beta\rangle = 0$, $\langle\delta\rangle \neq 0$), $\mu = 0.061$ and $\epsilon = 0.02$. (c) Chimera state ($\langle\sigma^\alpha\rangle \neq 0$ and $\langle\sigma^\beta\rangle = 0$), $\mu = 0.085$ and $\epsilon = 0.002$. (d) Desynchronized state ($\langle\sigma^\alpha\rangle \neq \langle\sigma^\beta\rangle \neq 0$), $\mu = 0.01$ and $\epsilon = 0.005$.

the populations do not affect the formation of chimeras with the reciprocal global coupling scheme of the system Eqs. (2.1)-(2.4).

2.4 Information flow between neuron populations in chimera states

We note that chimera states are probabilistic, in the sense that their occurrence depends on initial conditions. Once formed, chimera states are stable. We calculate the frequency f for occurrence of a chimera state, with one population synchronized and the other incoherent, over 100 realizations of random initial conditions for given parameter values. Figure 2.6 shows the frequency f as a function of the inter-population coupling parameter ϵ, for a fixed value of μ. We have

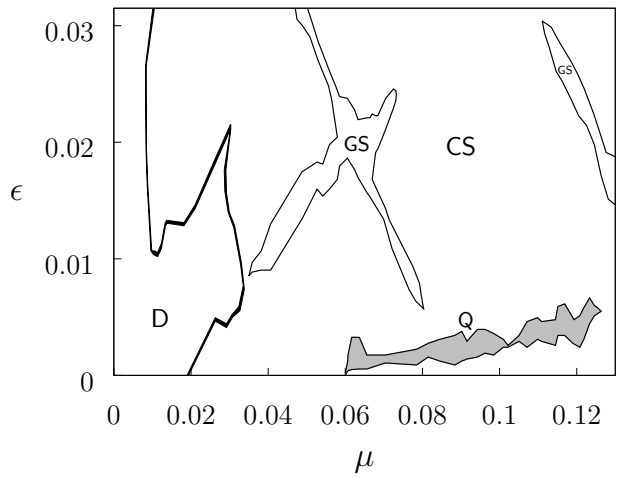

Figure 2.4: Phase diagram on the space of parameters (μ, ϵ) for the two population system, Eqs. (2.1)-(2.4), with local Rulkov dynamics, Eqs. (3.1)-(3.2). Fixed local parameters $\upsilon = 0.001$, $\varrho = 4.6$, $\gamma = 0.225$. Population sizes $N^{\alpha} = N^{\beta} = 500$. For each data point, the quantities $\langle \sigma^{\alpha} \rangle$, $\langle \sigma^{\beta} \rangle$, and $\langle \delta \rangle$ that characterize the different synchronization states are calculated over 1000 iterations after discarding 3000 transients, and averaged over 100 realizations of random initial conditions for each population. Labels CS, GS, Q, D, indicate the regions where collective synchronization states occur. The region where chimera states (Q) appear is colored in gray.

verified that the frequency to observe a chimera state does not change as the population sizes increase.

To elucidate the communication mechanisms between the neuron populations in a chimera state, we employ the information transfer introduced by Schreiber (Schreiber, 2000). Consider the dynamical variables y_t and x_t in an interacting system. Then, the information transfer from y_t to x_t is defined as (Schreiber, 2000)

$$T_{y \to x} = \sum_{x_{t+1}, x_t, y_t} p\left(x_{t+1}, x_t, y_t\right) \log \left[\frac{p\left(x_{t+1}, x_t, y_t\right) p\left(x_t\right)}{p\left(x_t, y_t\right) p\left(x_{t+1}, x_t\right)} \right], \tag{2.15}$$

where $p(x_t)$ is the probability distribution of the time series x_t, $p(x_t, y_t)$ is the joint probability distribution of x_t and y_t, and so on. The quantity $T_{y \to x}$ measures the degree of dependence of x on y; i.e., the information required to represent the value x_{t+1} from the knowledge of y_t. Note that the information transfer is non-symmetrical , i.e., $T_{y \to x} \neq T_{x \to y}$. When the two variables are synchronized, $x_t = y_t$; then $T_{y \to x} = 0$. An advantage of the information transfer is that it does not require

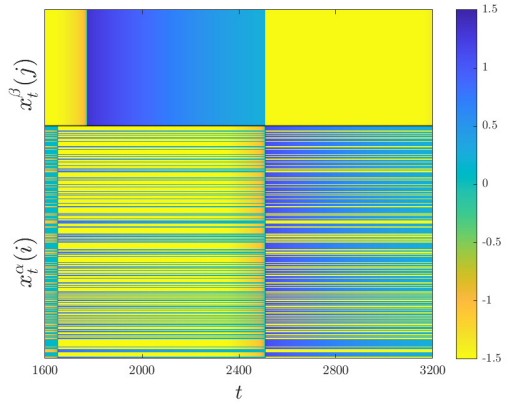

Figure 2.5: Spatiotemporal pattern for a chimera state in the system, Eqs. (2.1)-(2.4), with different population sizes $N^\alpha \neq N^\beta$. Fixed parameters $\upsilon = 0.001$, $\varrho = 4.6$, $\gamma = 0.225$. . (a) Rulkov map for local dynamics, Eqs. (3.1)-(3.2), with fixed parameters $\upsilon = 0.001$, $\varrho = 4.6$, $\gamma = 0.225$, $\mu = 0.12$, $\epsilon = 0.0032$, $N^\alpha = 400$, $N^\beta = 200$.

any knowledge of the dynamical system nor prior assumptions on data generation.

In our system, Eqs. (2.1)-(2.4), the two populations communicate through their respective mean fields. Thus, we consider the information transfer between the mean fields $\bar{X}_t^\alpha$ and $\bar{X}_t^\beta$ of populations α and β, respectively, when a chimera state is formed. We proceed as follows. For parameter values where a chimera state appears, after a transient time of 1500 iterations, we verify that a chimera state has formed and identify the synchronized and the desynchronized population with the labels S and D, respectively. Then, we take a time series of 1500 consecutive values for the mean fields of the synchronized and desynchronized populations, denoted by $\bar{X}_t^S$ and $\bar{X}_t^D$, respectively. From these data, we calculate the information transfers $T_{\bar{X}_t^S \to \bar{X}_t^D}$ and $T_{\bar{X}_t^D \to \bar{X}_t^S}$ by using the definition Eq. (2.15) (Behrendt et al., 2019).

Figure 2.7(a) shows the averaged quantities $T_{\bar{X}_t^D \to \bar{X}_t^S}$ and $T_{\bar{X}_t^S \to \bar{X}_t^D}$ as functions of the coupling ϵ in the region of parameters where chimera states arise. Figure 2.7(a) reveals that $T_{\bar{X}_t^D \to \bar{X}_t^S} > T_{\bar{X}_t^S \to \bar{X}_t^D}$, indicating a defined direction of the flow of information between the two neuron populations in chimera states, from the desynchronized population D to the synchronized one, S. We have also evaluated the statistical difference between the quantities $T_{\bar{X}_t^D \to \bar{X}_t^S}$ and $T_{\bar{X}_t^S \to \bar{X}_t^D}$ for different values of ϵ. To compare these quantities, we employ the Wilcoxon test which can

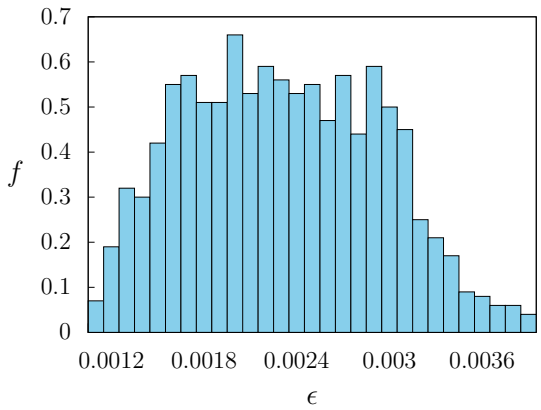

Figure 2.6: Frequency f for the emergence of a chimera state as a function of ϵ and a fixed value of $\mu = 0.09$ for the interacting populations system Eqs. (2.1)-(2.4). The frequency for observing a chimera state is calculated over 100 realizations of random and uniformly distributed initial conditions for each value of ϵ. Local dynamics is given by Rulkov maps, Eqs. (3.1)-(3.2), with fixed parameters $\upsilon = 0.001$, $\varrho = 4.6$, $\gamma = 0.225$. Population sizes are $N^{\alpha} = N^{\beta} = 500$.

be applied when the distribution of the difference between the two means of two samples cannot be assumed to be normally distributed. In Figure 2.7(b) we show the corresponding p-values as a function of ϵ. The dashed horizontal line marks the significance level 0.05. Very low p-values indicate that the differences between $T_{\bar{X}_t^D \to \bar{X}_t^S}$ and $T_{\bar{X}_t^S \to \bar{X}_t^D}$ are significant; therefore, Figure 2.7(b) provides a statistical evidence that $T_{\bar{X}_t^D \to \bar{X}_t^S} > T_{\bar{X}_t^S \to \bar{X}_t^D}$ in the range of parameters where chimera states appear.

Thus, a functional directionality emerges in the system despite the structural symmetry of our model, i.e., population D acts as the driver of population S in a chimera state. This result is relevant in the context of epileptic seizures that have been related to chimera states in brain dynamics (Andrzejak et al., 2016; Lainscsek et al., 2019). It has been found that there is a significant coupling direction in the oscillations from the thalamus to the seizure zone during epileptic seizures (Li et al., 2020).

We have verified that the formation of chimera states subsists as the sizes of the populations are increased by several orders of magnitude. In addition, we have investigated the influence of the size of the populations on the directionality of the flow of information in chimera states. Figure 2.8(a) shows the maximum

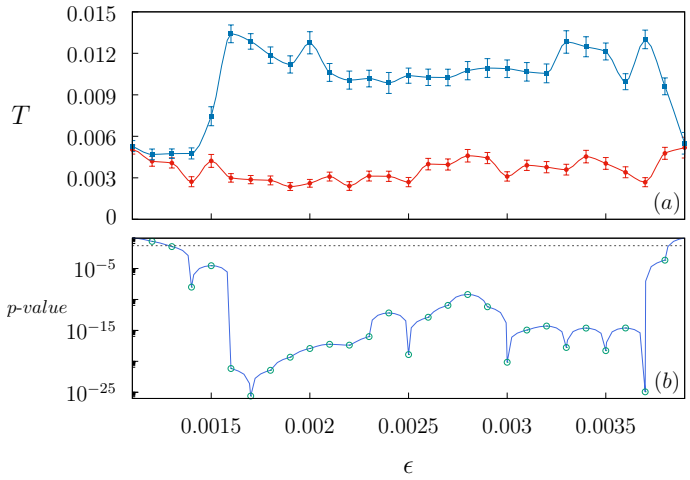

Figure 2.7: (a) Averaged $T_{\bar{X}_t^D \to \bar{X}_t^S}$ (squares, blue line) and $T_{\bar{X}_t^S \to \bar{X}_t^D}$ (circles, red line) in chimera states as functions of the coupling parameter ϵ, for the system Eqs. (2.1)-(2.4) with fixed $\mu = 0.09$. Local dynamics is given by Rulkov maps, Eqs. (3.1)-(3.2), with fixed parameters $\upsilon = 0.001$, $\varrho = 4.6$, $\gamma = 0.225$. Population sizes are $N^\alpha = N^\beta = 500$. Each data point of $T_{\bar{X}_t^D \to \bar{X}_t^S}$ and $T_{\bar{X}_t^S \to \bar{X}_t^D}$ is the average of 100 information transfer measures calculated over 100 realizations of initial conditions resulting in chimera states, where the synchronized and desynchronized populations S and D have been identified. Error bars represent the corresponding standard errors. (b) p-values obtained from the Wilcoxon test as a function of ϵ. The p-values characterize the statistical difference between the quantities $T_{\bar{X}_t^D \to \bar{X}_t^S}$ and $T_{\bar{X}_t^S \to \bar{X}_t^D}$. The dashed horizontal line signals the significance level 0.05.

frequency f_{max} for chimera states as a function of the population size $N^\alpha (= N^\beta)$. For each population size, we explore values (μ, ϵ) for which chimera state arise with a frequency calculated over 100 realizations of initial conditions. Then, we determine f_{max} as the maximum value of these frequencies.

In Fig. 2.8(b), for each population size $N^\alpha (= N^\beta)$ and its corresponding parameters (μ, ϵ) for which the frequency of finding a chimera state is maximum, we calculate the averaged $T_{\bar{X}_t^D \to \bar{X}_t^S}$ and $T_{\bar{X}_t^S \to \bar{X}_t^D}$ by proceeding similarly as in Fig. 2.7. The result $T_{\bar{X}_t^D \to \bar{X}_t^S} > T_{\bar{X}_t^S \to \bar{X}_t^D}$ persists independently of the system size. We have calculated the p-values obtained from the Wilcoxon test between the quantities $T_{\bar{X}_t^D \to \bar{X}_t^S}$ and $T_{\bar{X}_t^S \to \bar{X}_t^D}$ from Fig. 2.8(b). Figure 2.8(c) shows the corresponding p-values as a function of ϵ; they are much smaller than the significance level of 0.05. We note that the predominant direction of the information flow, from the desynchronized to the synchronized population, occurs even for the smallest possible populations of neurons ($N^\alpha = N^\beta = 2$). We have verified that the result

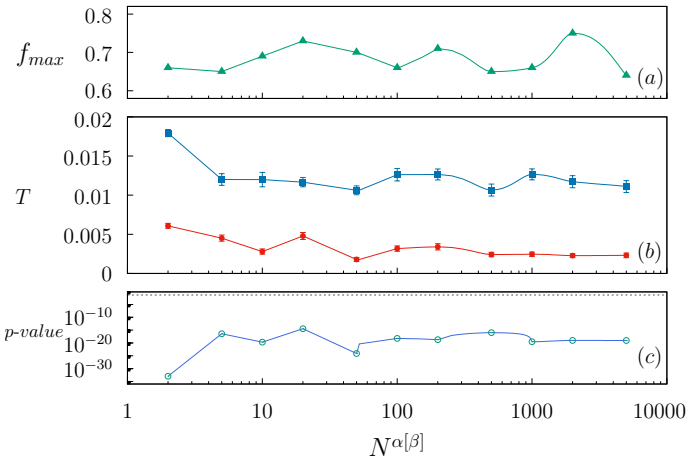

Figure 2.8: (a) Maximum frequency for chimera states as function of the population size $N^{\alpha}(=N^{\beta})$ in the system Eqs. (2.1)-(2.4). (b) Averaged $T_{\bar{X}_t^D \to \bar{X}_t^S}$ (squares, blue line) and $T_{\bar{X}_t^S \to \bar{X}_t^D}$ (circles, red line) in chimera states as functions of the population size $N^{\alpha}(=N^{\beta})$ in the system Eqs. (2.1)-(2.4). Error bars represent the corresponding standard errors. (c) p-values obtained from the Wilcoxon test as a function of ϵ. The p-values characterize the statistical difference between the quantities $T_{\bar{X}_t^D \to \bar{X}_t^S}$ and $T_{\bar{X}_t^S \to \bar{X}_t^D}$. The dashed horizontal line signals the significance level 0.05. Each data point on (a) and (b) corresponds to parameters (μ, ϵ) where a chimera state has maximum frequency to occur. Local dynamics is given by Rulkov maps, Eqs. (3.1)-(3.2), with fixed parameters $\upsilon = 0.001$, $\varrho = 4.6$, $\gamma = 0.225$.

$T_{\bar{X}_t^D \to \bar{X}_t^S} > T_{\bar{X}_t^S \to \bar{X}_t^D}$ prevails if different population partitions are employed.

In order to study whether the observed directionality in information transfer depends on whether the two populations of the system are coupled or not, we use a binomial test. This test was applied with a probability of success equal to 0.5, which corresponds to the null hypothesis that, in the absence of a directional bias, the probability of observing a higher information transfer in either direction is equally likely. Thus, any significant deviation from this probability would indicate the presence of a preferred directionality in the information transfer.

Multiple simulations with random initial conditions were run for a system of two coupled populations in a chimera state $(\mu = 0.09, \epsilon = 0.0023)$ and for a system of two uncoupled populations, where one is synchronized $(\mu = 0.01, \epsilon = 0)$ and the other is desynchronized $(\mu = 0.03, \epsilon = 0)$. For each simulation, the information transfer from the synchronized population to the desynchronized population, as well as the reverse, was computed.

For the coupled populations system, the information transfer was consistently biased toward the synchronized population. In 91% of the cases, the information transfer from the desynchronized population to the synchronized population was greater than in the reverse direction, with a very small p-value ($p < 2.2 \times 10^{-16}$), indicating strong statistical significance.

In contrast, for the uncoupled populations system, the results were less clear. In 58% of the simulations, the information transfer from the desynchronized population to the synchronized population was greater than in the reverse direction, with a p-value of 0.1332, suggesting that this difference was not statistically significant.

These results highlight that coupling between populations in a chimera state leads to a clear, statistically significant directionality in information transfer, while in uncoupled populations, no such significant bias was observed.

2.5 Conclusions

Coupled-map network models are computationally efficient, conceptually simple, and require few ingredients to study a variety of spatiotemporal processes, including synchronization phenomena, in complex systems and brain dynamics. In this article, we have investigated a system of two interacting populations of coupled maps subject to reciprocal global interactions, where the local units in each population exhibit neuron-like dynamics. We have focused on parameter values where the local maps exhibit chaotic spiking behavior. It has been found that chaotic dynamics in neurons leads to a greater diversity of responses that are relevant for neural computations (Rasmussen et al., 2017).

We have characterized four collective synchronization states emerging in the system: (i) complete synchronization, where the populations are synchronized to each other, (ii) generalized synchronization, where each population is synchronized, but no to the other, (iii) chimera state, where one population is synchronized and the other remains incoherent, and (iv) desynchronization, where both

populations are desynchronized.

Chimera states are probabilistic in the sense that their occurrence depends on initial conditions. On the parameter regions where the chimera states arise, the dynamics of the two-population system is multistable; i.e., several attractors coexist for the same parameter values. This behavior is typical of phase transition regions in dynamical systems. Chimeras represent an intermediate state between ordered and disordered phases.

We have found a well-defined direction of the flow of information in chimera states, from the desynchronized neuron population to the synchronized one. This result is independent of the population sizes or population partitions. The incoherent population functions as a driver of the coherent neuron population in a chimera state. This finding is consistent with previous reports where a measure of transfer entropy, applied to epileptic electrocorticography data, shows a significant coupling direction from the anterior nucleus of thalamus to the synchronized seizure onset zone during seizures (Li et al., 2020).

Although our results are obtained for specific neuron-map local dynamics, we expect that the drive-response causal relationship between the desynchronized and synchonized subsets persists for chimera states arising in general dynamical networks.

Models such as the presented here, where specific coupling parameters give rise to synchronization and chimera states, can provide insight to study phenomena such as unihemispheric sleep and brain disorders associated to alterations in the neural synchrony activity within and across brain areas (Wang and Liu, 2020). Neurological disorders, such as epilepsy, Alzheimer's and Parkinson's disease, and autism, have been related to abnormal neural synchronization patterns (Babiloni et al., 2017; Delbeuck et al., 2003; Dinstein et al., 2011; Jiruska et al., 2013; Uhlhaas and Singer, 2006).

Map-based neuron models are gaining recognition in the field of neuroscience, where they have been implemented in several studies (Nowotny et al., 2005; Sa-

yari et al., 2023; Yu et al., 2016). Although the two population model considered here is not specific in terms of biological plausibility, it yields the emergence of rich collective behavior that can be a useful tool in computational neuroscience. Future extensions of the two interacting population model proposed here should include the investigation of time delays, heterogeneity in the local dynamics, different connectivity networks, the similarity of collective states in driven and in autonomous systems, and the influence of external inputs.

Bibliography

Abrams, D. M., Mirollo, R., Strogatz, S. H., and Wiley, D. A. (2008). Solvable model for chimera states of coupled oscillators. *Physical Review Letters*, 101(8):084103.

Abrams, D. M. and Strogatz, S. H. (2004). Chimera states for coupled oscillators. *Physical Review Letters*, 93(17):174102.

Alvarez-Llamoza, O. and Cosenza, M. G. (2008). Generalized synchronization of chaos in autonomous systems. *Physical Review E*, 78(4):046216.

Andrzejak, R. G., Rummel, C., Mormann, F., and Schindler, K. (2016). All together now: Analogies between chimera state collapses and epileptic seizures. *Scientific Reports*, 6(1):23000.

Babiloni, C., Del Percio, C., Lizio, R., Noce, G., Cordone, S., Lopez, S., Soricelli, A., Ferri, R., Pascarelli, M. T., Nobili, F., et al. (2017). Abnormalities of cortical neural synchronization mechanisms in subjects with mild cognitive impairment due to alzheimer's and parkinson's diseases: an eeg study. *Journal of Alzheimer's Disease*, 59(1):339–358.

Barardi, A., Sancristóbal, B., and Garcia-Ojalvo, J. (2014). Phase-coherence transitions and communication in the gamma range between delay-coupled neuronal populations. *PLoS Computational Biology*, 10(7):e1003723.

Battaglia, D., Witt, A., Wolf, F., and Geisel, T. (2012). Dynamic effective connectivity of inter-areal brain circuits. *PLoS Computational Biology*, 8(3):e1002438.

Behrendt, S., Dimpfl, T., Peter, F. J., and Zimmermann, D. J. (2019). Rtransferentropy—quantifying information flow between different time series using effective transfer entropy. *SoftwareX*, 10:100265.

Bera, B. K., Ghosh, D., and Lakshmanan, M. (2016). Chimera states in bursting neurons. *Physical Review E*, 93(1):012205.

Bibbig, A., Traub, R. D., and Whittington, M. A. (2002). Long-range synchronization of γ and β oscillations and the plasticity of excitatory and inhibitory synapses: a network model. *Journal of Neurophysiology*, 88(4):1634–1654.

Bossomaier, T., Barnett, L., Harré, M., and Lizier, J. T. (2016). An introduction to transfer entropy: Information flow in complex systems. *Springer International Publishing*.

Breakspear, M. and Jirsa, V. K. (2007). Neuronal dynamics and brain connectivity. In *Handbook of Brain Connectivity*, pages 3–64. Springer.

Cardanobile, S. and Rotter, S. (2011). Emergent properties of interacting populations of spiking neurons. *Frontiers in Computational Neuroscience*, 5:59.

Cisneros, L., Jiménez, J., Cosenza, M. G., and Parravano, A. (2002). Information transfer and nontrivial collective behavior in chaotic coupled map networks. *Physical Review E*, 65(4):045204.

Cosenza, M. G. and Kapral, R. (1992). Coupled maps on fractal lattices. *Physical Review A*, 46(4):1850.

Delbeuck, X., Van der Linden, M., and Collette, F. (2003). Alzheimer'disease as a disconnection syndrome? *Neuropsychology Review*, 13:79–92.

Deschle, N., Daffertshofer, A., Battaglia, D., and Martens, E. A. (2019). Directed flow of information in chimera states. *Frontiers Appl. Math. Stat.*, 5:28.

Dinstein, I., Pierce, K., Eyler, L., Solso, S., Malach, R., Behrmann, M., and Courchesne, E. (2011). Disrupted neural synchronization in toddlers with autism. *Neuron*, 70(6):1218–1225.

Essaki Arumugam, E. M. and Spano, M. L. (2015). A chimeric path to neuronal synchronization. *Chaos: An Interdisciplinary Journal of Nonlinear Science*, 25(1):013107.

Glaze, T. A. and Bahar, S. (2021). Neural synchronization, chimera states and sleep asymmetry. *Frontiers in Network Physiology*, 1:734332.

Glaze, T. A., Lewis, S., and Bahar, S. (2016). Chimera states in a hodgkin-huxley model of thermally sensitive neurons. *Chaos: An Interdisciplinary Journal of Nonlinear Science*, 26(8):083119.

Goel, N. S., Maitra, S. C., and Montroll, E. W. (1971). On the volterra and other nonlinear models of interacting populations. *Reviews of Modern Physics*, 43(2):231.

Gomatam, J. (1974). A new model for interacting populations. *Bulletin of Mathematical Biology*, 36:347–353.

González-Avella, J. C., Cosenza, M. G., and San Miguel, M. (2014). Localized coherence in two interacting populations of social agents. *Physica A: Statistical Mechanics and its Applications*, 399:24–30.

Hizanidis, J., Kouvaris, N. E., Zamora-López, G., Díaz-Guilera, A., and Antonopoulos, C. G. (2016). Chimera-like states in modular neural networks. *Scientific Reports*, 6(1):19845.

Jiruska, P., De Curtis, M., Jefferys, J. G., Schevon, C. A., Schiff, S. J., and Schindler, K. (2013). Synchronization and desynchronization in epilepsy: controversies and hypotheses. *The Journal of Physiology*, 591(4):787–797.

Kaneko, K. (1984). Period-doubling of kink-antikink patterns, quasiperiodicity in antiferro-like structures and spatial intermittency in coupled logistic lattice: towards a prelude of a “field theory of chaos”. *Progress of Theoretical Physics*, 72(3):480–486.

Kaneko, K. (1993). Theory and applications of coupled map lattices. *Nonlinear Science: Theory and Applications*.

Kang, L., Tian, C., Huo, S., and Liu, Z. (2019). A two-layered brain network model and its chimera state. *Scientific reports*, 9(1):14389.

Kuramoto, Y. and Battogtokh, D. (2002). Coexistence of coherence and incoherence in nonlocally coupled phase oscillators. *Nonlinear Phenomena in Complex Systems*, 5:380.

Laing, C. R. (2010). Chimeras in networks of planar oscillators. *Physical Review E*, 81(6):066221.

Lainscsek, C., Rungratsameetaweemana, N., Cash, S. S., and Sejnowski, T. J. (2019). Cortical chimera states predict epileptic seizures. *Chaos: An Interdisciplinary Journal of Nonlinear Science*, 29(12):121106.

Lesku, J. A., Martinez-Gonzalez, D., and Rattenborg, N. C. (2009). Phylogeny and ontogeny of sleep. *The Neuroscience of Sleep*, 61:70.

Li, X., Xu, T., and Li, J. (2019). Synchronization and chimera states in a multilayer neuronal network with unidirectional interlayer links. *The European Physical Journal Special Topics*, 228:2419–2427.

Li, Z., Li, S., Yu, T., and Li, X. (2020). Measuring the coupling direction between neural oscillations with weighted symbolic transfer entropy. *Entropy*, 22(12):1442.

Magyar, A. and Collins, J. (2015). Two-population model for medial temporal lobe neurons: The vast majority are almost silent. *Physical Review E*, 92(1):012712.

Martens, E. A., Bick, C., and Panaggio, M. J. (2016). Chimera states in two populations with heterogeneous phase-lag. *Chaos: An Interdisciplinary Journal of Nonlinear Science*, 26(9).

Martens, E. A., Thutupalli, S., Fourriere, A., and Hallatschek, O. (2013). Chimera states in mechanical oscillator networks. *Proceedings of the National Academy of Sciences*, 110(26):10563–10567.

Maslennikov, O. V. and Nekorkin, V. I. (2014). Modular networks with delayed coupling: Synchronization and frequency control. *Physical Review E*, 90(1):012901.

Mehrabbeik, M., Parastesh, F., Ramadoss, J., Rajagopal, K., Namazi, H., and Jafari, S. (2021). Synchronization and chimera states in the network of electrochemically coupled memristive rulkov neuron maps. *Mathematical Biosciences and Engineering*, 18(6):9394–9409.

Montbrió, E., Kurths, J., and Blasius, B. (2004). Synchronization of two interacting populations of oscillators. *Physical Review E*, 70(5):056125.

Naze, S., Bernard, C., and Jirsa, V. (2015). Computational modeling of seizure dynamics using coupled neuronal networks: factors shaping epileptiform activity. *PLoS Computational Biology*, 11(5):e1004209.

Nowotny, T., Huerta, R., Abarbanel, H. D., and Rabinovich, M. I. (2005). Self-organization in the olfactory system: one shot odor recognition in insects. *Biological Cybernetics*, 93:436–446.

Omelchenko, I., Maistrenko, Y., Hövel, P., and Schöll, E. (2011). Loss of coherence in dynamical networks: Spatial chaos and chimera states. *Physical Review Letters*, 106(23):234102.

Omelchenko, I., Provata, A., Hizanidis, J., Schöll, E., and Hövel, P. (2015). Robustness of chimera states for coupled fitzhugh-nagumo oscillators. *Physical Review E*, 91(2):022917.

Panaggio, M. J. and Abrams, D. M. (2015). Chimera states: coexistence of coherence and incoherence in networks of coupled oscillators. *Nonlinearity*, 28(3):R67.

Patriarca, M. and Leppänen, T. (2004). Modeling language competition. *Physica A: Statistical Mechanics and its Applications*, 338(1-2):296–299.

Premalatha, K., Chandrasekar, V., Senthilvelan, M., and Lakshmanan, M. (2017). Chimeralike states in two distinct groups of identical populations of coupled stuart-landau oscillators. *Physical Review E*, 95(2):022208.

Rasmussen, R., Jensen, M. H., and Heltberg, M. L. (2017). Chaotic dynamics mediate brain state transitions, driven by changes in extracellular ion concentrations. *Cell Systems*, 5(6):591–603.

Rattenborg, N. C., Amlaner, C. J., and Lima, S. L. (2000). Behavioral, neurophysiological and evolutionary perspectives on unihemispheric sleep. *Neuroscience & Biobehavioral Reviews*, 24(8):817–842.

Rulkov, N. F. (2002). Modeling of spiking-bursting neural behavior using two-dimensional map. *Physical Review E*, 65(4):041922.

Rybalova, E., Bukh, A., Strelkova, G., and Anishchenko, V. (2019). Spiral and target wave chimeras in a 2d lattice of map-based neuron models. *Chaos: An Interdisciplinary Journal of Nonlinear Science*, 29(10).

Sayari, E., Gabrick, E. C., Borges, F. S., Cruziniani, F. E., Protachevicz, P. R., Iarosz, K. C., Szezech, J. D., and Batista, A. M. (2023). Analyzing bursting synchronization in structural connectivity matrix of a human brain under external pulsed currents. *Chaos: An Interdisciplinary Journal of Nonlinear Science*, 33(3).

Schreiber, T. (2000). Measuring information transfer. *Phys. Rev. Lett*, 85:461.

Shilnikov, A. L. and Rulkov, N. F. (2003). Origin of chaos in a two-dimensional map modeling spiking-bursting neural activity. *International Journal of Bifurcation and Chaos*, 13(11):3325–3340.

Stefanescu, R. A. and Jirsa, V. K. (2008). A low dimensional description of globally coupled heterogeneous neural networks of excitatory and inhibitory neurons. *PLoS Computational Biology*, 4(11):e1000219.

Tinsley, M. R., Nkomo, S., and Showalter, K. (2012). Chimera and phase-cluster states in populations of coupled chemical oscillators. *Nature Physics*, 8(9):662–665.

Uhlhaas, P. J. and Singer, W. (2006). Neural synchrony in brain disorders: relevance for cognitive dysfunctions and pathophysiology. *Neuron*, 52(1):155–168.

Ursino, M., Ricci, G., and Magosso, E. (2020). Transfer entropy as a measure of brain connectivity: A critical analysis with the help of neural mass models. *Frontiers in computational neuroscience*, 14:45.

Waller, I. and Kapral, R. (1984). Spatial and temporal structure in systems of coupled nonlinear oscillators. *Physical Review A*, 30(4):2047.

Wang, Z. and Liu, Z. (2020). A brief review of chimera state in empirical brain networks. *Frontiers in Physiology*, 11:724.

Wibral, M., Vicente, R., and Lindner, M. (2014). Directed information measures in neuroscience. *Springer Berlin*.

Yu, L., De Mazancourt, M., Hess, A., Ashadi, F. R., Klein, I., Mal, H., Courbage, M., and Mangin, L. (2016). Functional connectivity and information flow of the respiratory neural network in chronic obstructive pulmonary disease. *Human Brain Mapping*, 37(8):2736–2754.

Zakharova, A. (2020). Chimera patterns in networks. *Springer*.

3. Impact of cortical connectivity on phase-amplitude coupling and metastability in neural networks

Abstract

Neural oscillations in the human cortex play a critical role in cognitive functions by facilitating communication across different brain regions. Recent computational models have explored the dynamics of these oscillations, often focusing on network architecture and the balance between excitatory and inhibitory interactions. However, the relationship between brain connectivity patterns and the emergence of complex oscillatory features, such as phase-amplitude coupling (PAC), remains underexplored. In this study, we propose a map-based neuron model that incorporates real cortical connectivity derived from human brain tissue. We examine how this network structure influences the emergence of PAC and the metastability of the system. Using the modulation index (MI) to quantify PAC and spectral entropy to measure the metastability of the signal, we compare a network with biologically realistic connectivity to a randomly permuted model. Our results demonstrate that PAC emerges more strongly in networks based on real cortical tissue connectivity, with a broader range of oscillatory frequencies and higher spectral entropy, suggesting greater network flexibility and adaptability. These findings highlight the importance of cortex network structure in the generation of complex neural oscillations, which may underlie a variety of cognitive processes.

3.1 Introduction

Neural oscillations in the human cortex follow distinct patterns that are crucial for cognitive functions (Buzsaki and Draguhn, 2004). These oscillations facilitate communication both within and between brain regions, ensuring precise temporal coordination in processes such as memory, attention, and cognition (Roux and Uhlhaas, 2014; Soto-Icaza et al., 2019; Ward, 2003). Evidence for neural oscillations in cognitive processing is supported not only by experiments but also by computational and mathematical models (Doelling and Assaneo, 2021; Ermentrout and Chow, 2002). In fact, these models highlight the role of various factors such as coupling strength (Ghosh et al., 2020), the balance between excitatory

and inhibitory synapses for global neuronal activity dynamics (Trousdale et al., 2012), and network architecture (Shao and Ostojic, 2023; Zang et al., 2024).

Neural oscillations, while often resembling simple sinusoidal patterns, are fundamentally complex phenomena shaped by the intricate interplay between intrinsic cellular properties and neuronal circuits (Buzsaki and Draguhn, 2004; Cole and Voytek, 2017). These oscillations manifest across various spatial scales, reflecting the combined influence of network-level connectivity and the dynamics of individual neurons and synapses (Wang, 2010). Recent studies have shed light on the critical role of cortical layer organization, where specific connectivity patterns within these layers contribute to the generation of distinct oscillatory frequency bands (Mendoza-Halliday et al., 2024). Therefore, understanding these patterns requires a deeper exploration of how cortical connectivity underpins the emergence of oscillatory activity, bridging structural organization with complex oscillatory features. To address this gap, we investigate the emergence of phase-amplitude coupling and metastability as key oscillatory features, shaped by human cortical connectivity patterns. In this way, we consider the reported bias for excitatory neurons to connect more frequently with other neurons within the same layer, as well as the stronger excitatory-inhibitory coupling observed within neurons (Campagnola et al., 2022; Galakhova et al., 2022; Sadeh and Clopath, 2021).

Phase-amplitude coupling (PAC) is a specific form of cross-frequency coupling in which a low-frequency rhythm modulates the amplitude of a high-frequency rhythm (Salimpour and Anderson, 2019). This relationship between the phase of a low-frequency oscillation and the amplitude of a higher-frequency oscillation, can occur either within a single neuronal population or across different populations (Chehelcheraghi et al., 2016; Salimpour et al., 2024).

Although PAC has been detected in different mammals and within various brain regions, including humans (Axmacher et al., 2010; Billeke et al., 2020), monkeys

(Esghaei et al., 2015; Lakatos et al., 2005) and rats (van Wingerden et al., 2014), mechanisms for PAC generation are still to be understood. However, it is proposed that coordinated activity between different types of neurons, particularly excitatory pyramidal neurons and inhibitory interneurons, is important for the emergence of PAC (Chehelcheraghi et al., 2016). Furthermore, it is suggested that the degree of PAC is significantly influenced by the structure of the neural network (Salimpour et al., 2024).

Oscillatory features such as PAC facilitates spontaneous transitions between different states of neural activity (Sase and Kitajo, 2021). This metastable condition allows neural dynamics to remain adaptable, enabling groups of neurons to reconfigure and respond effectively to both internal and external stimuli (Tognoli and Kelso, 2014). Such flexibility is essential for the brain to adapt its oscillatory patterns as needed, supporting a variety of cognitive functions efficiently (Cabral et al., 2022).

Brain activity is inherently variable, characterized by a dynamic interplay between regular rhythms and unpredictable fluctuations (Garrett et al., 2013). Entropy, which quantifies this complexity, can be used for measuring irregularity or unpredictability of a signal, offering insight into the brain's functional state (Kosciessa et al., 2020). Higher entropy can be associated with the development and specialization of certain areas of the brain for specific cognitive functions, suggesting that increased neural variability reflects a more flexible and adaptive processing capacity, leading to more advanced and efficient cognitive function (Amalric and Cantlon, 2023).

Entropy-based metrics can be classified according to the signal domain. In the frequency domain, spectral entropy can be used to compute the entropy of the signal. Spectral entropy is a metric that can be used as a proxy for metastability (Torres et al., 2024). In addition, it has been used for analyzing neural signals, regardless of their nonlinear behavior, and to obtain important information from

neuronal networks (Helakari et al., 2019; Kapucu et al., 2016; Tost et al., 2024)

While recent studies have shown that PAC is a key feature of neural networks, observed in both in vivo and in vitro conditions, the neural connectivity properties within these networks remain under-explored (Salimpour et al., 2024). Therefore, the aim of this study is to contribute to better understand the neural mechanism by which, key oscillatory features such a PAC, emerges from a specific network topology. We hypothesized that complex oscillatory features depends on specific patterns of cortical connectivity on neural populations. To test this hypotheses we measure PAC by calculating the modulation index described by Canolty et al. (Canolty et al., 2006), and metastability by computing the spectral entropy based on Shannon entropy. These metrics are calculated in a map-based neuron model that incorporates connectivity patterns typical of human cortical tissue. Unlike traditional differential equation-based models, where each equation represents the dynamics of an entire neural population, our approach uses map-based models to represent the dynamics of individual neurons within the population. This novel approach, to our knowledge, has not been previously employed in PAC studies.

In recent years, map-based neuron models have emerged as a computationally efficient and conceptually straightforward alternative for studying complex neuronal behaviors (Girardi-Schappo et al., 2013; Ibarz et al., 2011). By capturing the dynamics of individual neurons, these models align with recent theoretical frameworks suggesting that population rhythms can arise from the irregular firing patterns of single neurons (Wang, 2010). This makes map-based models particularly valuable for investigating how individual neuronal activity contributes to emergent oscillatory phenomena at the population level (Márquez-Rodríguez et al., 2024).

The paper is structured as follows: first, we present our model describing local dynamics as map-based neurons and the network connectivity based on connection probabilities derived from human cortex. Subsequently, we introduce the metrics to calculate PAC and metastability. Then, we reveal the simulations numerical

results, indicating dominant oscillatory frequencies, MI and spectral entropy, as a functions of coupling parameters. Finally, we have the discussion and conclusions.

3.2 Model and methods

3.2.1 Local dynamics

Discrete dynamical systems, also known as iterative maps, have begun to receive attention in the last decades as valid phenomenological models for representing the firing behavior of neurons (Ibarz et al., 2011). Map-based modeling, in addition to allowing the replication of different firing patterns for specific cell types, can be used to study oscillations and synchronization in circuits or networks of neurons (Rulkov and Bazhenov, 2008).

The two-dimensional map model proposed by Rulkov (2002), is introduced here to represent local dynamics given as:

$$x_{t+1} = f(x_t, y_t + \beta_t), \tag{3.1}$$

$$y_{t+1} = y_t - \mu(x_t + 1) + \mu\sigma + \mu\sigma_t; \tag{3.2}$$

where x_t and y_t represent the fast and slow dynamical variables, respectively, with parameter μ $(0 < \mu \ll 1)$ acting as the separation of time scales between variables. σ is a control parameter used to define the resting potential of the model neuron. $\beta_t = \beta^e I_t^{\text{ext}}$ and $\sigma_t = \sigma^e I_t^{\text{ext}}$ are input variables that represent synaptic and other external currents injected into the neuron. In this way, I^{ext} accounts for the sum of the external currents.

The piece-wise nonlinear function $f(x_t, y_t + \beta_t)$ has the form

$$f(x_t, y_t + \beta_t) = \begin{cases} \alpha(1 - x_t)^{-1} + y_t + \beta_t & \text{if} \quad x \leq 0, \\ \alpha + y_t + \beta_t & \text{if} \quad 0 < x_t < \alpha + y_t + \beta_t \text{ and } x_{t-1} \leq 0; \\ -1 & \text{if} \quad x_t \geq \alpha + y_t + \beta_t \text{ or } x_{t-1} > 0. \end{cases} \tag{3.3}$$

Based on the parameter values, as reported in (Rulkov et al., 2004), the model described by Eqs. (3.1)-(3.2)-(3.3) can represent the dynamics of various types of neurons. In this study, we use $\alpha = 3.5$, $\mu = 0.0005$, $\sigma = 0.06$, $\sigma^e = 1$, $\beta^e = 0.133$ as the fixed parameter values for excitatory neurons and $\alpha = 3.8$, $y = -2.9$, $\beta^e = 0.1$ for inhibitory neurons. Additionally, the dynamics of inhibitory neurons take into account a hyperpolarization current I^{hp} generated by the action of each spike, defined as:

$$I_{t+1}^{\text{hp}} = (0.85) \cdot I_t^{\text{hp}} - \begin{cases} 0.27 & \text{if the n-th iteration carries a spike;} \\ 0 & \text{otherwise,} \end{cases} \tag{3.4}$$

Synaptic inputs can be modeled as iterative maps as well. Adapted from the Hodgkin-Huxley model, synaptic currents I^{syn} can be written as (Rulkov et al., 2004):

$$I_{t+1}^{\text{syn}} = \gamma_s I_t^{\text{syn}} - \begin{cases} g_s(x_t^{\text{post}} - x_{rp}) & \text{if} \quad 0 < x_t^{\text{pre}} < \alpha + y_t^{\text{pre}} + \beta_t^{\text{pre}} \text{ and } x_{t-1}^{\text{pre}} \leq 0; \\ 0 & \text{otherwise,} \end{cases} \tag{3.5}$$

where γ_s is a parameter that controls the relaxation rate of the synaptic current and g_s is the strength of synaptic coupling, with index $s = \text{exc or inh}$, depending on the type of synapse: excitatory or inhibitory, respectively. Parameter x_{rp} represents the reversal potential. Here, as reported in (Rulkov et al., 2004), we use fixed

values $\gamma_{\text{exc}} = 0.6$, $x_{\text{rp}} = 0.0$ for excitatory synapses, and $\gamma_{\text{inh}} = 0.96$, $x_{\text{rp}} = -1.1$ for inhibitory synapses.

Considering that the variable x_t on the map defined in Eqs. (3.1)-(3.2) is dimensionless, it is possible to convert it to millivolt units using the following relation (Rulkov and Bazhenov, 2008):

$$V_t = \frac{-50\text{mV}}{1 - \sqrt{\alpha}} \cdot x_t \tag{3.6}$$

As for the time unit, the time interval between one iteration and the next for the map is 0.5 ms. This time is also the sampling frequency.

3.2.2 Network connectivity

To ensure that our model incorporates connectivity based on real biological patterns, we define neuron connections using a connection probability matrix M_p derived from cortical tissue in humans (Campagnola et al., 2022). In this way, the model considers a tendency for excitatory neurons to connect more frequently with neurons within the same layer than with neurons from different layers, as occurs in the cortex (Campagnola et al., 2022; Galakhova et al., 2022). Also, the probability matrix M_p takes into account a stronger excitatory-inhibitory coupling within neurons, which is relevant for information processing (Sadeh and Clopath, 2021). A detailed diagram of the connectivity probabilities can be seen in Figure 3.1.

In matrix $M_p \in R^{6\times6}$, rows and columns from 1 to 5 correspond to excitatory neurons located in layers L2, L3a, L3b, L4, and L5, respectively, while row and column 6 correspond to inhibitory neurons. Thus, an element $M_{p,ij}$ indicates the probability that a neuron from type indicated in row i synapses with a neuron from type indicated in column j.

For a network of size N, an extended adjacency matrix $M_a \in \{0,1\}^{N\times N}$ is created from M_p. Thus, to create M_a, each neuron is first labeled as I = {1, 2, . . . , 6}, where labels 1 to 5 correspond to a specific cortex layer, and label 6

corresponds to inhibitory neurons. This assignment is done such that 20% of the total neurons are labeled as 6, while labels from 1 to 5 are equally distributed among the remaining 80%. Then, each element $M_{a,ij}$ has an assigned connection probability p_{ij}, which depends on the labels l_i and l_j assigned to elements i and j, respectively. This probability is found at the position (l_i, l_j) in the matrix M_p. To assess whether a connection exists from neuron i to neuron j, a uniform random number κ is generated in the range $[0, 1]$. A link is established if $\kappa < p_{ij}$.

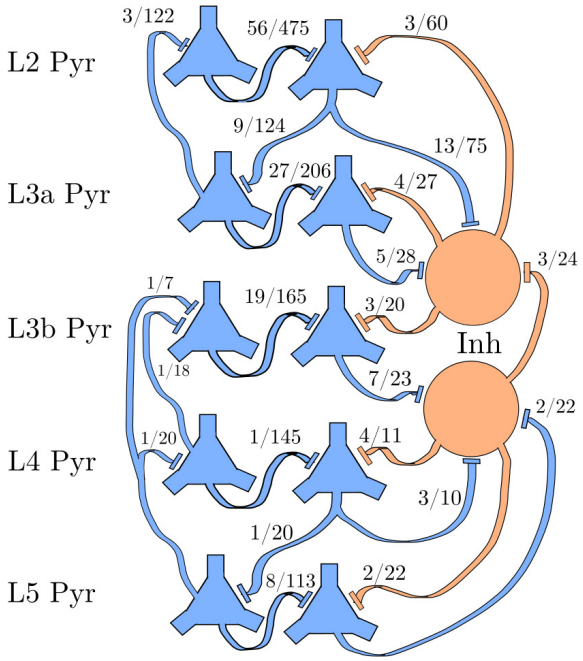

Figure 3.1: **Connection probability derived from human cortical tissue.** Schematic representation of pyramidal neurons (blue) organized in cortical layers alongside inhibitory neurons (orange), showing the probability of synaptic connections within and across layers, as well as between excitatory and inhibitory neurons.

3.2.3 Phase-amplitude coupling

To measure the coupling between the high-frequency amplitude (f_{amp}) and low-frequency phase (f_{ph}), we use a modulation index (MI) as described by Canolty et al. (Canolty et al., 2006), and implemented through the MATLAB toolbox developed by Onslow et al. (Onslow et al., 2011). The complex-valued composite signal is constructed by combining the high-frequency amplitude envelope $A_{\text{famp}}(t)$

and the phase of the low-frequency signal $\theta_{\text{fph}}(t)$ as follows:

$$Z_{\text{fph, famp}}(t) = A_{\text{famp}}(t) \cdot e^{i\theta_{\text{fph}}(t)} \tag{3.7}$$

This composite signal is analyzed in the complex plane. If the average value of this signal is non-zero, assuming the phase distribution is uniform, it suggests a systematic co-occurrence of specific amplitude and phase values over time.

The MI is then calculated as the absolute value of the average of this composite signal:

$$\text{MI}_{\text{fph, famp}} = |\text{average}(Z_{\text{fph, famp}}(t))| \tag{3.8}$$

A non-zero MI indicates a coupling between the amplitude and phase, with the magnitude of the MI reflecting the strength of the phase-amplitude coupling. This approach is sensitive to the joint distribution of amplitude and phase, providing a robust metric for analyzing phase-amplitude relationships across different frequency bands.

3.2.4 Spectral entropy

To calculate the spectral entropy of a signal, we first apply the Fast Fourier Transform (FFT) to obtain its frequency domain representation X_{dft}. We then take the positive half of the spectrum and compute the power spectral density (PSD) by normalizing the FFT by the sampling frequency F_s and the total number of points N:

$$\text{PSD(i)} = \frac{1}{F_s \cdot N} \cdot |X_{dft}(i)|^2 \tag{3.9}$$

where i denotes the i-th frequency component. Since we took only the positive half of the spectrum, we then multiply the PSD by a factor of 2, to conserve the total power (excluding zero frequency (DC) and the Nyquist frequency). Finally, we compute the spectral entropy SE directly from the PSD using the Shannon

entropy:

$$\text{SE} = -\sum_{i} \text{PSD(i)} \log_{10}(\text{PSD(i)}) \tag{3.10}$$

This calculation allows us to express the power distribution of the signal across different frequency components in probabilistic terms, ultimately yielding the spectral entropy of the signal.

3.3 Results

3.3.1 Influence of excitatory and inhibitory synaptic coupling on network frequency

To investigate how the coupling parameters g_{exc} and g_{inh} affect the dominant oscillatory frequency in a network of neurons, we compute the maximum frequency (f_{max}) of the signal obtained from averaging the activity of excitatory neurons only. This is done by first generating an extended adjacency matrix M_a for a population of N neurons, and then obtaining the signal for each pair of coupling parameters $(g_{\text{exc}}, g_{\text{inh}}) \in [0, 12]$. To remove low-frequency noise, the averaged signal is centered at zero by subtracting its mean over time. To ensure the signal is comparable across conditions, it is normalized by its maximum value. The frequency spectrum of the normalized signal is then computed using the Fast Fourier Transform (FFT). The maximum frequency is identified by locating the peak in the power spectrum, which reflects the dominant oscillation frequency of the network. This process is repeated across multiple simulations for each parameter combination, and the average of the maximum frequencies is used to represent the observed distribution for each coupling configuration.

In order to ensure that the results obtained are not a product of chance, we proposed a random model, in which the connection probability matrix M_p is randomly permuted. Then, the extended matrix M_a is obtained and the process to compute the dominant oscillatory frequency is done as described before. The resulting distributions of the maximum oscillatory frequency for both the network based on

cortical tissue connectivity and the random model are presented and compared in Figure 3.2.

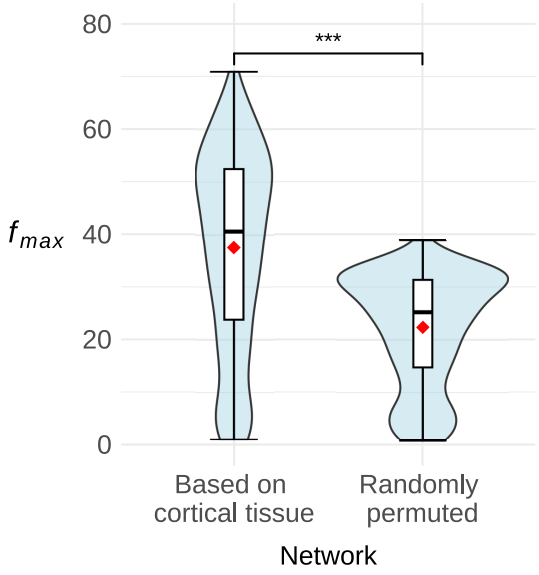

Figure 3.2: **Dominant oscillatory frequency as a function of coupling parameters.** Violin plots showing the distribution of the maximum oscillatory frequency (f_{max}) for a network based on cortical connectivity (left) and a randomly connected network (right), as a function of excitatory and inhibitory coupling parameters (g_{exc}, g_{inh}). For each data point, f_{max} is calculated for a unique parameter combination over 3000 iterations after discarding 3500 transients, and averaged over 100 realizations of random initial conditions for the phases of the depolarization pulses. Red points indicate the mean. Population size $N = 100$, with $N_{\text{exc}} = 80$ and $N_{\text{inh}} = 20$. A Wilcoxon rank-sum test ($p = 1.48 \times 10^{-82}$) compares the maximum frequency distributions between networks.

3.3.2 Emergence of Phase-amplitude coupling based on network structure

As shown in Figure Fig 3.2, the model, using a network topology based on real connectivity patterns, is capable of generating frequencies across a broad range, from delta to gamma. Since phase-amplitude coupling (PAC) requires at least one slow and one fast frequency component (Chehelcheraghi et al., 2016), we explore the emergence of PAC patterns in this context. To study PAC, we use the modulation index MI as a proxy, while systematically varying the coupling parameters $(g_{\text{exc}}, g_{\text{inh}})$. Based on the averaged signal of the excitatory neuron activity, we calculated the MI in the theta frequency range (4-8 Hz) for the modulating signal, and in the gamma frequency range (40-80 Hz) for the PAC signal. These frequency

bands are particularly important as their coupling is involved in different cognitive information processing, including speech processing (Lizarazu et al., 2019), working memory (Daume et al., 2024), and learning (Tort et al., 2009). The results obtained after exploring the values of g_s in the interval $[0, 12]$ are presented in Figure 3.3. Fig 3.3(a) illustrates that when the adjacency matrix of the network is derived from the connection probability matrix based on cortical tissue in humans, a region of favorable values for phase-amplitude coupling emerges, characterized by MI ≥ 3, in this case. Conversely, Fig 3.3(b), which presents a random model of this network, reveals the absence of such a favorable region.

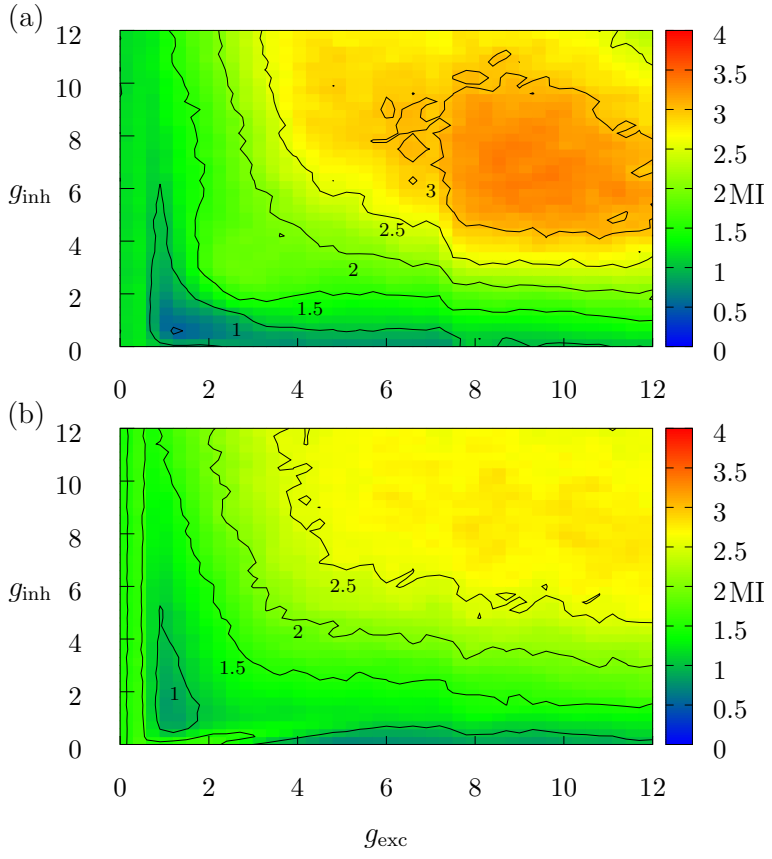

Figure 3.3: **Phase diagram on the space of coupling parameters $(g_{\text{exc}}, g_{\text{inh}})$ in terms of the modulation index.** (a) Network connectivity based on cortical tissue. (b) Random model featuring a randomly permuted version of the network connectivity probabilities in (a). For each data point in each Figure, MI is calculated for a unique parameter combination over 3000 iterations after discarding 3500 transients, and averaged over 100 realizations of random initial conditions for the phases of the depolarization pulses. Population size $N = 100$, with $N_{\text{exc}} = 80$ and $N_{\text{inh}} = 20$.

3.3.3 Metastability

To better understand the role of metastability in facilitating spontaneous transitions between neural states, we investigated the coupling parameter space of the system where PAC was explored. In this context, we calculated spectral entropy for the same signal used in the MI computation, across different coupling parameters $(g_{\text{exc}}, g_{\text{inh}})$. The results are portrayed in Figure 3.4.

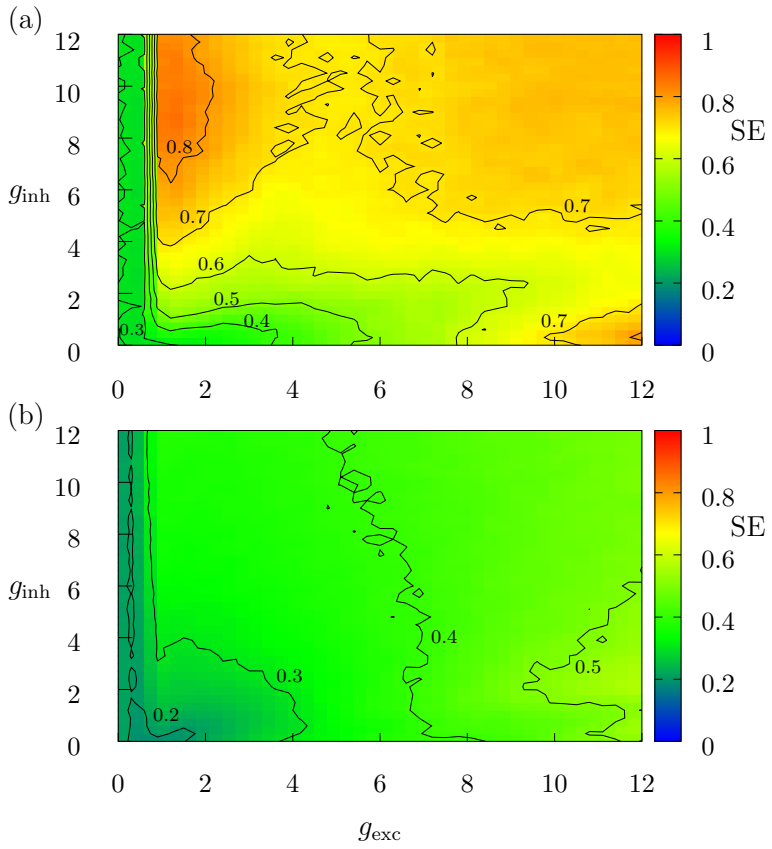

Figure 3.4: **Phase diagram on the espace of coupling parameters $(g_{\text{exc}}, g_{\text{inh}})$ in terms of the spectral entropy.** (a) Network connectivity based on cortical tissue. (b) Random model featuring a randomly permuted version of the network connectivity probabilities in (a). For each data point in each Figure, SE is calculated for a unique parameter combination over 3000 iterations after discarding 3500 transients, and averaged over 100 realizations of random initial conditions for the phases of the depolarization pulses. Population size $N = 100$, with $N_{\text{exc}} = 80$ and $N_{\text{inh}} = 20$.

Fig 3.4(a) shows that when the adjacency matrix of the network is derived from the connection probability matrix based on cortical tissue in humans, exhibits higher spectral entropy values, indicating a high level of complexity and a

diverse frequency distribution. In contrast, Fig 3.4(b), which presents the calculations from a signal generated in a random model, shows lower spectral entropy values, suggesting a more predictable signal with a concentrated frequency distribution. By comparing Fig 3.3(a) with Fig 3.4(a), it can be observed that the region with higher MI values coincides with a region of higher SE values. In contrast, by comparing Fig 3.3(b) with Fig 3.4(b), no clear regions of concordance are observed.

3.3.4 Topological roles of excitatory and inhibitory neurons in cortical connectivity

To gain a deeper understanding of which factors in cortical connectivity are leading to higher PAC and metastability, we explored the relevance of the two types of neurons in the network: excitatory and inhibitory. Specifically, we used degree and betweenness as metrics for a quick inspection. Table 3.1 shows the results obtained from the network generated with cortical connectivity probabilities and the network generated with randomly permuted probabilities. The results show that, in the case of the network with cortical connectivity, inhibitory neurons have a more influential position within the network, as opposed to when random permutations are used.

	Cortical connectivity		Randomly permuted	
Metric	E (Mean)	I (Mean)	E (Mean)	I (Mean)
In-degree	5.87	19.28	7.87	7.37
Out-degree	6.87	15.26	7.88	7.32
Betweenness	69.75	410.78	178.55	148.07

Table 3.1: Results obtained after averaging 100 different networks generated from the cortical connectivity probability matrix, and from a randomly permuted probability matrix.

3.4 Discussion and Conclusions

Understanding the emergence of complex oscillatory features in neural networks remains a central challenge in neuroscience. In this paper, we have studied the relationship between a network structure of human cortical tissue and the

emergence of complex oscillatory features using a map-based neuron model. Our results demonstrate that our model is capable of generating multi-band frequency components, which is key feature for accurately modeling PAC dynamics (Chehelcheraghi et al., 2016). Moreover, we have found that networks based on real cortical connectivity patterns, exhibit a stronger PAC than networks with randomly permuted connectivity. This finding suggests that the underlying structure of the neural network, including the tendency for excitatory neurons to connect preferentially within the same cortical layer, plays a crucial role in the generation of PAC. These results are consistent with other studies which suggest that the degree of PAC is significantly influenced by the structure of the neural network (Salimpour et al., 2024).

The connectivity biases between cortical layers suggest that inter-layer connectivity and the interaction between oscillations at different frequencies play a critical role in the generation of PAC. Experimental observations in the visual cortex of monkeys have shown that faster oscillations, such as gamma, tend to emerge from different cortical layers than slower oscillations like alpha (Van Kerkoerle et al., 2014). Similarly, studies in the auditory cortex indicate that attention modulates frequency tuning in a layer-specific manner, with response suppression in supragranular layers and enhancement in granular and infragranular layers (O'Connell et al., 2014). This evidence emphasizes the significance of exploring how cross-layer interactions contribute to the emergence of complex oscillatory features, highlighting the relevance of our model in exploring these dynamics further.

We found that the network's metastability, measured by spectral entropy, is enhanced in the model when the connectivity is biologically realistic based from the human cortex. Cortical metastability arises from a specific structural organization that supports complex and flexible functional dynamics (La Camera et al., 2019; Sporns et al., 2002). Furthermore, other studies have emphasized that cortical regions form a dynamical cortical core, which operates at maximum metastability

and plays a crucial role in the brain's global network dynamics (Deco et al., 2017).

In our model, we simulate the network dynamics in its spontaneous state, without any external perturbations, focusing exclusively on its intrinsic connectivity and the emergent behavior of the system. This approach offers insights into the brain's resting state. Empirical studies have shown that even when at rest, cortical regions maintains a state of maximum metastability (Deco et al., 2017). Theories suggest that metastability in the resting state allows the brain to explore its full range of possible configurations, with the highest probability of switching between network states, based on the brain's fixed structural connections (Alderson et al., 2020; Ponce-Alvarez et al., 2015). Notably, PAC has been observed in spontaneous activity, between thalamic alpha oscillations and cortical gamma activity, during the resting state using MEG recordings, highlighting the role of phasic inhibition in coordinating cortical activity Roux et al. (2013).

Our study explores the coupling parameter space, identifying regions where the highest values for PAC and metastability coincide. This observation is supported by the findings of Sase et al. (Sase and Kitajo, 2021), whose work is among the first to examine experimentally, the relationship between PAC dynamics and metastability. They reported transitions between delta-alpha PAC states, highlighting how these shifts between metastable brain states are facilitated by PAC. Our results align with theirs, as we also observe that the regions with the highest PAC values coincide with those exhibiting high values of spectral entropy.

By examining the relationship between network topology and oscillatory dynamics, this study reveals that the structural properties of cortical networks are crucial in shaping PAC and metastability. The use of map-based models proves to be an excellent tool for studying these dynamics, offering computational efficiency and a straightforward approach to exploring complex neuronal oscillations.

Phase-amplitude coupling (PAC) is increasingly recognized as a ubiquitous feature of brain activity, potentially playing a fundamental role in both basic and

higher-order information processing. While many existing models separate excitatory and inhibitory populations into distinct dynamic equations Chehelcheraghi et al. (2016), the model presented here takes a different approach. It explores PAC as an emergent property within a single population of neurons, emphasizing the importance of network structure and synaptic interactions. This perspective highlights how oscillatory dynamics, shaped by local and long-range synaptic connections, can coordinate distributed neural ensembles involved in perception, attention, memory, and action. By capturing these emergent patterns, the model offers valuable insights into the mechanisms underlying PAC and its role in large-scale brain communication.

Future work could expand on this study by incorporating a more detailed exploration of oscillatory dynamics across different cortical layers, the influence of external stimuli, and the interactions between distinct neuron populations.

Bibliography

Alderson, T. H., Bokde, A. L., Kelso, J. S., Maguire, L., and Coyle, D. (2020). Metastable neural dynamics underlies cognitive performance across multiple behavioural paradigms. *Human brain mapping*, 41(12):3212–3234.

Amalric, M. and Cantlon, J. F. (2023). Entropy, complexity, and maturity in children's neural responses to naturalistic video lessons. *Cortex*, 163:14–25.

Axmacher, N., Henseler, M. M., Jensen, O., Weinreich, I., Elger, C. E., and Fell, J. (2010). Cross-frequency coupling supports multi-item working memory in the human hippocampus. *Proceedings of the National Academy of Sciences*, 107(7):3228–3233.

Billeke, P., Ossandon, T., Perrone-Bertolotti, M., Kahane, P., Bastin, J., Jerbi, K., Lachaux, J.-P., and Fuentealba, P. (2020). Human anterior insula encodes performance feedback and relays prediction error to the medial prefrontal cortex. *Cerebral Cortex*, 30(7):4011–4025.

Buzsaki, G. and Draguhn, A. (2004). Neuronal oscillations in cortical networks. *science*, 304(5679):1926–1929.

Cabral, J., Castaldo, F., Vohryzek, J., Litvak, V., Bick, C., Lambiotte, R., Friston, K., Kringelbach, M. L., and Deco, G. (2022). Metastable oscillatory modes emerge from synchronization in the brain spacetime connectome. *Communications Physics*, 5(1):184.

Campagnola, L., Seeman, S. C., Chartrand, T., Kim, L., Hoggarth, A., Gamlin, C., Ito, S., Trinh, J., Davoudian, P., Radaelli, C., et al. (2022). Local connectivity and synaptic dynamics in mouse and human neocortex. *Science*, 375(6585):eabj5861.

Canolty, R. T., Edwards, E., Dalal, S. S., Soltani, M., Nagarajan, S. S., Kirsch, H. E., Berger, M. S., Barbaro, N. M., and Knight, R. T. (2006). High gamma power is phase-locked to theta oscillations in human neocortex. *science*, 313(5793):1626–1628.

Chehelcheraghi, M., Nakatani, C., Steur, E., and van Leeuwen, C. (2016). A neural mass model of phase–amplitude coupling. *Biological cybernetics*, 110(2-3):171–192.

Cole, S. R. and Voytek, B. (2017). Brain oscillations and the importance of waveform shape. *Trends in cognitive sciences*, 21(2):137–149.

Daume, J., Kamiński, J., Schjetnan, A. G., Salimpour, Y., Khan, U., Kyzar, M., Reed, C. M., Anderson, W. S., Valiante, T. A., Mamelak, A. N., et al. (2024). Control of working memory by phase–amplitude coupling of human hippocampal neurons. *Nature*, pages 1–9.

Deco, G., Kringelbach, M. L., Jirsa, V. K., and Ritter, P. (2017). The dynamics of resting fluctuations in the brain: metastability and its dynamical cortical core. *Scientific reports*, 7(1):3095.

Doelling, K. B. and Assaneo, M. F. (2021). Neural oscillations are a start toward understanding brain activity rather than the end. *PLoS biology*, 19(5):e3001234.

Ermentrout, G. B. and Chow, C. C. (2002). Modeling neural oscillations. *Physiology & behavior*, 77(4-5):629–633.

Esghaei, M., Daliri, M. R., and Treue, S. (2015). Attention decreases phase-amplitude coupling, enhancing stimulus discriminability in cortical area mt. *Frontiers in neural circuits*, 9:82.

Galakhova, A., Hunt, S., Wilbers, R., Heyer, D. B., De Kock, C., Mansvelder, H. D., and Goriounova, N. A. (2022). Evolution of cortical neurons supporting human cognition. *Trends in cognitive sciences*, 26(11):909–922.

Garrett, D. D., Samanez-Larkin, G. R., MacDonald, S. W., Lindenberger, U., McIntosh, A. R., and Grady, C. L. (2013). Moment-to-moment brain signal variability: a next frontier in human brain mapping? *Neuroscience & Biobehavioral Reviews*, 37(4):610–624.

Ghosh, S., Mondal, A., Ji, P., Mishra, A., Dana, S. K., Antonopoulos, C. G., and Hens, C. (2020). Emergence of mixed mode oscillations in random networks of diverse excitable neurons: The role of neighbors and electrical coupling. *Frontiers in Computational Neuroscience*, 14:49.

Girardi-Schappo, M., Tragtenberg, M. H. R., and Kinouchi, O. (2013). A brief history of excitable map-based neurons and neural networks. *Journal of neuroscience methods*, 220(2):116–130.

Helakari, H., Kananen, J., Huotari, N., Raitamaa, L., Tuovinen, T., Borchardt, V., Rasila, A., Raatikainen, V., Starck, T., Hautaniemi, T., et al. (2019). Spectral entropy indicates electrophysiological and hemodynamic changes in drug-resistant epilepsy–a multimodal mreg study. *NeuroImage: Clinical*, 22:101763.

Ibarz, B., Casado, J. M., and Sanjuán, M. A. (2011). Map-based models in neuronal dynamics. *Physics reports*, 501(1-2):1–74.

Kapucu, F. E., Välkki, I., Mikkonen, J. E., Leone, C., Lenk, K., Tanskanen, J. M., and Hyttinen, J. A. (2016). Spectral entropy based neuronal network synchronization analysis based on microelectrode array measurements. *Frontiers in Computational Neuroscience*, 10:112.

Kosciessa, J. Q., Kloosterman, N. A., and Garrett, D. D. (2020). Standard multiscale entropy reflects neural dynamics at mismatched temporal scales: What's signal irregularity got to do with it? *PLoS computational biology*, 16(5):e1007885.

La Camera, G., Fontanini, A., and Mazzucato, L. (2019). Cortical computations via metastable activity. *Current opinion in neurobiology*, 58:37–45.

Lakatos, P., Shah, A. S., Knuth, K. H., Ulbert, I., Karmos, G., and Schroeder, C. E. (2005). An oscillatory hierarchy controlling neuronal excitability and stimulus processing in the auditory cortex. *Journal of neurophysiology*, 94(3):1904–1911.

Lizarazu, M., Lallier, M., and Molinaro, N. (2019). Phase- amplitude coupling between theta and gamma oscillations adapts to speech rate. *Annals of the new York Academy of Sciences*, 1453(1):140–152.

Márquez-Rodríguez, V. J., Tucci, K., and Cosenza, M. G. (2024). Chimera states and information transfer in interacting populations of map-based neurons. *Neural Computing and Applications*, 36(29):18151–18159.

Mendoza-Halliday, D., Major, A. J., Lee, N., Lichtenfeld, M. J., Carlson, B., Mitchell, B., Meng, P. D., Xiong, Y., Westerberg, J. A., Jia, X., et al. (2024). A ubiquitous spectrolaminar motif of local field potential power across the primate cortex. *Nature Neuroscience*, 27(3):547–560.

O'Connell, M. N., Barczak, A., Schroeder, C. E., and Lakatos, P. (2014). Layer specific sharpening of frequency tuning by selective attention in primary auditory cortex. *Journal of Neuroscience*, 34(49):16496–16508.

Onslow, A. C., Bogacz, R., and Jones, M. W. (2011). Quantifying phase–amplitude coupling in neuronal network oscillations. *Progress in biophysics and molecular biology*, 105(1-2):49–57.

Ponce-Alvarez, A., Deco, G., Hagmann, P., Romani, G. L., Mantini, D., and Corbetta, M. (2015). Resting-state temporal synchronization networks emerge from connectivity topology and heterogeneity. *PLoS computational biology*, 11(2):e1004100.

Roux, F. and Uhlhaas, P. J. (2014). Working memory and neural oscillations: alpha–gamma versus theta–gamma codes for distinct wm information? *Trends in cognitive sciences*, 18(1):16–25.

Roux, F., Wibral, M., Singer, W., Aru, J., and Uhlhaas, P. J. (2013). The phase of thalamic alpha activity modulates cortical gamma-band activity: evidence from resting-state meg recordings. *Journal of Neuroscience*, 33(45):17827–17835.

Rulkov, N. F. (2002). Modeling of spiking-bursting neural behavior using two-dimensional map. *Physical Review E*, 65(4):041922.

Rulkov, N. F. and Bazhenov, M. (2008). Oscillations and synchrony in large-scale cortical network models. *Journal of Biological Physics*, 34(3):279–299.

Rulkov, N. F., Timofeev, I., and Bazhenov, M. (2004). Oscillations in large-scale cortical networks: map-based model. *Journal of computational neuroscience*, 17(2):203–223.

Sadeh, S. and Clopath, C. (2021). Excitatory-inhibitory balance modulates the formation and dynamics of neuronal assemblies in cortical networks. *Science advances*, 7(45):eabg8411.

Salimpour, Y. and Anderson, W. S. (2019). Cross-frequency coupling based neuromodulation for treating neurological disorders. *Frontiers in neuroscience*, 13:125.

Salimpour, Y., Anderson, W. S., Dastgheyb, R., Liu, S., Ming, G.-l., Song, H., Maragakis, N. J., and Habela, C. W. (2024). Phase-amplitude coupling detection and analysis of human 2-dimensional neural cultures in multi-well microelectrode array in vitro. *Journal of Neuroscience Methods*, 407:110127.

Sase, T. and Kitajo, K. (2021). The metastable brain associated with autistic-like traits of typically developing individuals. *PLOS Computational Biology*, 17(4):e1008929.

Shao, Y. and Ostojic, S. (2023). Relating local connectivity and global dynamics in recurrent excitatory-inhibitory networks. *PLOS Computational Biology*, 19(1):e1010855.

Soto-Icaza, P., Vargas, L., Aboitiz, F., and Billeke, P. (2019). Beta oscillations precede joint attention and correlate with mentalization in typical development and autism. *Cortex*, 113:210–228.

Sporns, O., Tononi, G., and Edelman, G. (2002). Theoretical neuroanatomy and the connectivity of the cerebral cortex. *Behavioural brain research*, 135(1-2):69–74.

Tognoli, E. and Kelso, J. S. (2014). The metastable brain. *Neuron*, 81(1):35–48.

Torres, F. A., Otero, M., Lea-Carnall, C. A., Cabral, J., Weinstein, A., and El-Deredy, W. (2024). Emergence of multiple spontaneous coherent subnetworks from a single configuration of human connectome coupled oscillators model. *Scientific Reports*, 14(1):30726.

Tort, A. B., Komorowski, R. W., Manns, J. R., Kopell, N. J., and Eichenbaum, H. (2009). Theta–gamma coupling increases during the learning of item–context associations. *Proceedings of the National Academy of Sciences*, 106(49):20942–20947.

Tost, A., Bachiller, A., Medina-Rivera, I., Romero, S., Serna, L.-Y., Rojas-Martínez, M., García-Cazorla, Á., and Mañanas, M. Á. (2024). Repetitive active and passive cognitive stimulations induce eeg changes in patients with rett syndrome. *Pediatric Research*, pages 1–12.

Trousdale, J., Hu, Y., Shea-Brown, E., and Josić, K. (2012). Impact of network structure and cellular response on spike time correlations. *PLoS computational biology*, 8(3):e1002408.

Van Kerkoerle, T., Self, M. W., Dagnino, B., Gariel-Mathis, M.-A., Poort, J., Van Der Togt, C., and Roelfsema, P. R. (2014). Alpha and gamma oscillations characterize feedback and feedforward processing in monkey visual cortex. *Proceedings of the National Academy of Sciences*, 111(40):14332–14341.

van Wingerden, M., van der Meij, R., Kalenscher, T., Maris, E., and Pennartz, C. M. (2014). Phase-amplitude coupling in rat orbitofrontal cortex discriminates between correct and incorrect decisions during associative learning. *Journal of Neuroscience*, 34(2):493–505.

Wang, X.-J. (2010). Neurophysiological and computational principles of cortical rhythms in cognition. *Physiological reviews*, 90(3):1195–1268.

Ward, L. M. (2003). Synchronous neural oscillations and cognitive processes. *Trends in cognitive sciences*, 7(12):553–559.

Zang, J., Liu, S., Helson, P., and Kumar, A. (2024). Structural constraints on the emergence of oscillations in multi-population neural networks. *Elife*, 12:RP88777.

4. Conclusions

The findings of this thesis contribute to a deeper understanding of how oscillatory states emerge in neuronal populations, with a particular focus on the information flow between neural populations and the role of connectivity patterns in shaping complex oscillatory features. By employing computational models, we have explored the mechanisms underlying these phenomena, shedding light on both fundamental aspects of brain function and their potential implications for neurological disorders.

Our approach followed two key stages. First, we developed a model consisting of two interacting populations of map-based neurons coupled through a mean-field interaction. Building upon the insights gained from this initial framework, we then introduced a second model with greater biological plausibility, allowing us to investigate how specific neural circuit properties influence emergent oscillatory features.

In the first stage, we showed that systems of interacting neuron-like chaotic maps can exhibit diverse synchronization states, including chimera states, which bridge ordered and disordered dynamics. Our results reveal that these states are characterized by a directional flow of information, with desynchronized populations acting as drivers for synchronized ones. This insight aligns with research on neurological conditions such as epilepsy and autism, where abnormal synchronization patterns are observed, suggesting that understanding such causal relationships could help to understand these disorders.

In the second stage, we examined how biologically realistic cortical connec-

tivity influences the emergence of complex oscillatory features such as PAC and metastability. Our findings indicate that incorporating realistic connectivity patterns enhances these phenomena, highlighting the importance of layer-specific cortical interactions. These results are consistent with research on cortical layer organization, where specific connectivity patterns shape distinct oscillatory frequency bands. Furthermore, such structural organization plays a critical role in shaping flexible and adaptive neural dynamics, aligning with empirical evidence that links metastability to the brain's resting state and its capacity to transition between network configurations.

The main contribution of this thesis lies in the development of a framework based on population models of map-based neurons to understand the emergence of complex neuronal oscillatory patterns. Developing neuronal computational models is essential not only for designing better experiments but also for uncovering the underlying reasons behind observed experimental results. Map-based neuron models have proven to be both computationally efficient and conceptually accessible, serving as powerful tools to bridge individual neuronal activity with large-scale network dynamics and reveal key mechanisms driving complex oscillatory behaviors. Notably, this work contributes by employing map-based neuron models to study information flow in chimera states and the emergence of PAC, a novel approach that, to the best of our knowledge, has not been previously explored.

Based on these insights, several extensions of this work arise as future research challenges. For example, refining models' connectivity parameters using real data can help explore whether they accurately replicate patterns observed in resting-state activity and epileptic controls. In this way, parameters such as the intensity of excitatory and inhibitory synapses can be fine-tuned to capture transitions between physiological and pathological states.

Another important aspect to explore is the influence of external inputs. Stimulation through TMS or tDCS is an active research area that still requires further studies to achieve precise and controlled modulation of neuronal activity. In this

context, applying rectangular or sinusoidal pulses to different proportions of neurons in our models could provide valuable insights into their impact on network and circuit dynamics.